UNIVERSITÀ
degli STUDI
di CATANIA

Università degli Studi di Catania

Dipartimento di Scienze Biomediche e Biotecnologiche "Biometech"

Dottorato di Ricerca Internazionale in Neurosceinze - XXXI Ciclo

Technological innovations in multimodal management of glioblastoma: from nano-drugs to imaging guided surgery and supra-maximal resection.

Candidate: Dr. Francesco Certo

Tutor: Prof. Giovanni Puglisi

Co-Tutor: Prof. Giuseppe Barbagallo

Index

6. **In vivo experiments on temozolomide**

a. *Methods*

    i. *Model of glioma-bearing rats*

    ii. *In vivo brain distribution of NPs*

    iii. *In vivo anti-glioma activity*

b. *Results*

    i. *TMZ brain concentration*

    ii. *Evaluation of anti-glioma activity*

    iii. *Evaluation of anti-glioma activity*

7. **Discussion**

a. *Strategies to improve surgical and clinical outcome*

b. *Strategies to increase the effectiveness of adjuvant therapy: nanotechnologies to cross BBB*

c. *Theranostic*

d. *Personalized medicine*

e. *Preclinical phase and clinical trials*

8. **Limitation and perspectives**

9. **Conclusions**

1. Introduction

Primary brain tumors are a major cause of morbidity and mortality in the United States (1). Approximately one-third of tumors are malignant and the remaining are benign or borderline malignant. High-grade glioma, in particular glioblastoma, management is a great challenge for both neurosurgeons and patients. More than 45% of CNS primary malignant tumours are glioblastoma and their 5 year-survival is only 5% on average. Although biomolecular differences between glioblastoma IDH-WT and IDH-mutant might account for different outcomes, treatment strategies, including surgical EOR, chemiotherapy and radiotherapy, are currently considered important factors associated with PFS and OS (2-5).

1.1 Image-guided surgery for management of Glioblastoma

In order to increase tumor extent of resection and reduce complications, several intraoperative technologies, like neuronavigation, neuromonitoring, fluorescence-guidance, intraoperative Magnetic Resonance (i-MR), intraoperative Computed Tomography (i-CT) and intraoperative Ultrasound (i-US) have been variably investigated and applied to brain tumor surgery with promising results. However, most of them are usually used independently and clinical practice revealed several limitations and pitfalls related to each one of them (6-14).
Neuronavigation is routinely used during brain tumors resection. However, the brain shift-phenomenon, caused by surgical retraction, blood and cerebrospinal fluid (CSF) loss as well as by tumor removal itself, is responsible for progressive loss of navigation accuracy and may limit its use, particularly in cases of large or deeply sited lesions. As a result, the use of preoperative imaging-based neuronavigation becomes less reliable during surgery and intraoperative, *real time* image-guided surgery is gaining momentum to compensate for brain shift, increase tumor resection accuracy and improve post-operative outcome with regard to OS and QOL.
Effectiveness of 5 aminolevulinic acid (5-ALA) fluorescence-guided surgery in increasing HGGs EOR has been proven (15). 5-ALA fluorescence-guided surgery, albeit useful to achieve maximal or supramaximal resection, may be associated with increased risk of eloquent areas injury, particularly in tumors extensively infiltrating the white matter. In such cases, cortical and

subcortical electrical stimulation can aid to pursue a balanced compromise between function preservation and surgical radicality. Neuromonitoring has been proposed also in brain metastases surgery with controversial results (6).

With regard to intraoperative imaging, for more than a decade i-MR was considered the most accurate tool to assess EOR in glioma surgery. High quality images allowing brain parenchyma and residual contrast-enhancing, or abnormal, tissue visualization, without exposure to ionizing radiation, is i-MR main advantage. Unfortunately, both i-MR machines and the entire MR-compatible operating theatre are expensive and yet limited to a small number of neurosurgical centers worldwide (8,9).

The use of i-CT has been reported in cases of tumors spreading to the brain surface, in transsphenoidal surgery and, more recently, during surgery for intra-axial tumors, like low-grade glioma (10-12). Although i-CT-related radiation dose is usually low, it may still limit the use of this technology; moreover, minimal residual tumor can be undetectable on CT scan. Conversely, benefits of i-CT include correction for brain shift during neuronavigation (similarly to i-MR), localization of contrast-enhancing tumor and associated necrotic areas inadvertently left behind after microsurgical resection as well as early identification of complications, particularly intraoperative hemorrhage. Yet, it is also important to highlight the wider financial and logistic accessibility of i-CT for many centers as well as the intraoperative time gain, particularly when a portable i-CT scanner is used (10).

Considering advantages and limitations of each of the above tools, efforts are currently made to identify their most useful and effective combination in brain tumor surgery, in order to achieve both maximal and safe tumor EOR and improved patients′ OS and QOL.

1.2 *Impact of extent of tumor resection on survival*

Sanai *et al.* demonstrated that tumour EOR ≥95% is a positive prognostic factor (16). Currently, researchers are also focusing on options allowing more accurate visualization of the tumour mass, to let surgeons achieve a EOR nearing 100%. Moreover, in the past few years supramarginal tumour resection for LGG, DLGG and metastases, as a strategy providing improved PFS e OS, has been reported (17).

How to achieve improved outcome results in HGGs is the quest of modern research, considering that usually glioblastoma recurrence takes place within two centimeters around the initial tumor margins.

Currently, standard preoperative MRI protocols allow tumour volume measurement and its edges delineation: they give volumetric and anatomical information about the intracranial mass and guide tumour excision through the use of neuronavigation. Tumor edges are defined on T1-contrast enhanced sequences, assuming that contrast enhancement is due to BBB disruption driven by tumour infiltration. Currently, standard tumor excision is based on such altered-BBB edges delineation, preserving the surrounding eloquent areas with electrophysiological mapping. However , in addition to T1-weighted sequences, an important role is played by T2w-FLAIR images, which help in determining tumor structural margins, due to CSF suppression and improved sulcal anatomy visualization. Yet, FLAIR images usually show tumors larger than T1-weighted sequences, and they also depict peritumoral areas where it′s supposed that remaining tumour cells are located. But specificity of FLAIR sequences in delineating tumour extension is reduced by their limitations in distinguishing lesion edges (with real tumour infiltration) from perilesional oedema (18). In addition, similarly to other preoperative imaging techniques, MRI accuracy is also plagued by brain shift (19).

Following Stummer′s *et al.* studies (15) the use of 5-ALA fluorescence has become another useful and commonly used intraoperative tool, in association with neuronavigation, during brain tumor surgery. Since the spread of 5-ALA fluorescence use, many surgeons observed the presence of fluorescent areas beyond tumor edges seen on gadolinium-enhanced, T1-weighted MRI. Despite the high PPV (positive predictive value) of 5-ALA in recognising tumour tissue, different technical features and problems may lower its NPV (negative predictive value). In particular, the higher the distance from the main tumour bulk, the lower the tumor cell density and hence fluorescence intensity. Moreover, during surgery presence of blood in the surgical field, depth of tumour infiltration and hidden areas not reachable by microscope light can obstruct surgeon′s view and ability to detect tumor tissue (10,15).

T2-weighted FLAIR sequences and 5-ALA fluorescence both improve tumour visualization, beyond the T1-weighted, contrast-enhanced, area. Both FLAIR images and 5-ALA fluorescence are likely to also include in the tumour volume those peritumoral (i.e. tumor peripheral) areas where small tumor cell nests hide; and these nests are known to be associated with the high frequency of tumor recurrences and the consequent low survival expectancy.

1.3 *After surgery: adjuvant therapy with Temozolomide and role of nanotechnologies*

The treatment protocol for these tumors includes, in addition to the surgical treatment, the combination of adjuvant chemo- and radiotherapy. The drug typically used in the standard chemotherapeutic protocol is temozolomide, an imidazole derivative that is taken orally for five days a month for six months. Recent evidences of literature, however, suggest a possible greater efficacy of the drug, for prolonged doses over 6 months provided by the standard protocol (20). Pharmacokinetic and pharmacodynamic studies on temozolomide have found that this molecule has a very short plasma half-life (about 1.8 hours), so that an adequate concentration in glial cells can only be reached following the systemic administration of high doses. In addition, parenteral administration of this drug is normally avoided, as the preparation for intravenous administration (lyophilized powder) has been reported as a possible cause of allergic reactions and haemolysis. Recently, laboratory experiments have been reported aiming to realize nanopharmaceuticals compounds by including the temozolomide molecule in liposomal carriers in order to increase the half-life of the drug and its ability to effectively cross the blood-brain barrier. The first pre-clinical experiments with liposomal vectors have reported encouraging results, however, the literature analysis shows a marked lack of data on the possibility of using temozolomide in combination with other engineered vectors (21). Furthermore, no studies have yet emerged to investigate the possibility of administering temozolomide via different routes of administration. The blood-brain barrier (BBB) and the blood-CSF barrier (BCB) represent natural barriers that limit the spread and concentration of drugs within the central nervous system (CNS). The main physiological function of these barriers is to preserve the nervous structures from possible insults of pathogens of various kinds, constituting a filter for exchanges between the blood side and the CNS (22). Systemic administration of drugs targeting the CNS must therefore take this limitation into account. BEE and BEL restrict the transport of CNS active drugs through two main methods: for hydrophilic drugs that cannot permeate the cell wall, the so-called "paracellular" transport through the tight junctions of BEE is highly limited by the same dimensions of molecules, whereby only the smallest molecules can transit through the BEE; for lipophilic drugs that are able to cross the cell membrane, the "transcellular" crossing of the BEE is limited by the active action of proteins such as the P-glycoprotein (pgp) or the proteins of the family of the multridrug resistance-related proteins (MRRp) that are located on the surface of the cell membrane. The transcellular way for the penetration of drugs within the CNS is therefore limited only to molecules that can interact with specific membrane transporters that facilitate its transit. The possibility of exploiting alternative routes of administration for drugs that are difficult to penetrate BEE has led to the development of intra-thecal administration systems (22). However, these methods, besides being invasive and presenting risks associated with the administration procedure, make the CNS vulnerable to the penetration of

pathogens or harmful agents.
Starting from these premises, it has emerged in recent years, the need to identify safe and reproducible routes of administration for those drugs that are difficult to cross the blood-brain barrier. During the last decade, several research fields have been carried out in the neuropharmacological field, in order to identify possible carriers for a series of drugs used in various pathological conditions of the CNS. These researches aimed to identify engineered vectors prepared with the help of nanotechnology methods able to facilitate the penetration of the CNS both of molecules already used for the treatment of neurodegenerative or neoplastic disorders and of drugs whose efficacy it is instead limited by the presence of BBB and / or BCB.
The studies conducted on the engineered vectors have associated the pre-clinical and clinical research lines on alternative routes to the traditional ones for CNS active drugs. In this sense, the intranasal administration of drugs able to exploit the nose-brain pathway seems to be a safe and effective method, which is showing promising results according to what emerges from the first scientific experiences in this regard (22,23).
From the studies reported in the literature on the route of intranasal administration of neurotropic drugs, it is clear that there are undeniable advantages linked to the nose-to-brain pathway (23). Firstly, the bioavailability of the drugs administered through this path is increased by the lack of the effect of the "first pass". Secondly, the nose-brain pathway seems to bypass the transit of the molecules through the blood-brain barrier, exploiting the pathway provided by the nerve endings of the cranial nerves (in particular the olfactory and trigeminal) and thus creating direct access to the brain. SNC. Finally, the rapid absorption of the drug through the nasal mucosa seems to guarantee an immediate efficacy of the drug in the face of a very minimally invasive and safe administration modality

2. Aims

The objective of this thesis is the definition of a neuro-oncological protocol, to be reserved for patients with glioblastoma, which can establish a therapeutic path that starts with a safe and effective surgery and continues with a pharmacological treatment that may lead to the limitations of current antitumor therapy schemes.

Two main research lines have been conducted, with these purposes: the first one, essentially clinical , has been analysed in two consecutive studies, first retrospectively, then prospectively, the results of the application of an intraoperative imaging protocol that foresees the use of Advanced neuronavigation, intraoperative fluorescence and intraoperative CT. The second line of research was instead based on the attempt to obtain a pharmacological preparation which provided for the combination of temozolomide with nano-vectors, able to increase its antiblastic efficacy and to increase its chances of delivery at the intracranial level.

3. Retrospective clinical study on intraoperative imaging

3.1 Methods

A total of 25 consecutive patients (Group A), including 15 men, with a mean age of 58 years (range, 30-80 years), were operated on between July 2010 and July 2014 at the Department of Neurosurgery, Policlinico University Hospital, Catania, Italy, because of a suspected diagnosis of HGG. In all cases, image-guided surgery was also performed using portable i-CT. Preoperatively, MRI was performed according to institu- tional preoperative imaging protocol, including volumetric gadolinium- enhanced T1, T2, fluid-attenuated inversion recovery sequences, spectroscopic analysis, diffusion-weighted images, and perfusion- weighted images; in all but 6 cases, a contrast-enhanced CT scan was also obtained. Two patients presented with recurrent neoplasms, and 4 patients had multifocal neoplasms.

Group A patients were compared with a historical consecutive series of 25 patients (Group B) (13 males), with a mean age of 61 years (range, 8-82 years), with glioblastomas; the latter group underwent surgery before the introduction of portable CT at our institution assisted with 5-ALA and neuronavigation only. The same preoperative imaging studies as in Group A were performed in Group B. All patients in both groups were operated on by the same 3 surgeons. We included in the current study 2 consecutive series of patients treated at the same institution. The absence of bias related to differences of demographic data in both groups was statistically verified. 5-ALA fluorescence guidance and neuronavigation were used in all patients in both groups. We performed an intended biopsy only in 1 patient in Group A. Afterward, in Group A patients, a postcontrast i-

CT scan was obtained to assess intraoperatively the EOTR; in the only case of a biopsy, intraoperative CT control was useful to verify the exact site of sampling and to rule out early hemorrhagic complications. However, this patient was excluded from the current analysis. Pre- and postoperative Karnofsky performance status (KPS) score was assessed in both patient groups as well as overall survival (OS) and progression-free survival (PFS) data. Pre- and postoperative KPS score was measured 1 day before surgery and on the day of discharge (usually postoperative day 5). In Group A patients, we used an 8-slice small-bore portable CT scanner (CereTom; NeuroLogica, Danvers, Massachusetts); a StealthStation S7 (Medtronic, Minneapolis, Minnesota) neuronavigation system was used for surgery in both groups.

3.2 Results

In Group A, histopathology revealed 21 cases (84%) of glioblastoma, 2 cases of anaplastic astrocytoma, and 2 of anaplastic oligodendroglioma, respectively. Conversely, all Group B tumors were diagnosed as glioblastomas.

In 8 of 25 Group A patients (32%), i-CT revealed intra- operatively unrecognized residual tumor; in 4 of these patients (16%) harboring a multifocal neoplasm, it helped to further resect the just seen neoplastic foci detached from the main tumor nodule and not detected by 5-ALA. In such cases, additional navigation-assisted resection was performed after importing the updated i-CT images into the navigation system (Table 1). Further exploration of those areas highlighted by the i-CT scan confirmed the presence of highly fluorescent tumor tissue. Correlation between residual tumor documented by i-CT and 5-ALA was evaluated using neuronavigation. Indeed, i-CT images were not affected by brain shift, and the enhancing tissue could be detected using the navigation probe. In all cases requiring further resection, we detected tumor fluorescent tissue covered by necrotic non-fluorescent tumor or normal nonfluorescent white matter. Moreover, neuronavigation documented in all cases a positive correlation between highly fluorescent tissue and i-CT contrast- enhancing areas.

TABLE 1. Characteristics of Patients Undergoing Intraoperative Computed Tomography During Surgery for High-grade Gliomas[a]

Patient No.	Sex	Age, y	No. of i-CT Scans	Further Resection	Final Resection[b]	Hystopathology	Tumor Location	Preoperative KPS Score	Postoperative KPS Score
1	F	47	2	No	GTR	GBM	Left frontal	80	90
2	M	73	3	Yes	GTR	GBM	Right frontal	50	40
3	F	43	3	No	GTR	GBM	Cerebellum	50	20
4	M	70	2	No	GTR	GBM	Left rolandic	60	60
5	F	59	2	Yes	GTR	GBM	Right frontal	70	90
6	M	32	2	No	GTR	GBM	Right rolandic	90	90
7	F	75	2	No	GTR	GBM	Right parietal	60	60
8	M	30	2	Yes	GTR	GBM	Right insular	90	100
9	M	71	2	No	Biopsy	AA	Left frontal	70	80
10	M	57	2	Yes	GTR	GBM	Left frontal	80	80
11	F	55	2	No	GTR[c]	GBM	Right multicentric	60	80
12	F	60	2	Yes	GTR[c]	GBM	Left multicentric	40	40
13	M	56	3	No	GTR	GBM	Left temporal	90	80
14	M	58	2	No	GTR	GBM	Right insular	80	100
15	M	62	2	No	GTR	GBM	Left parietal	80	80
16	F	80	2	No	GTR	GBM	Left frontoinsular	50	50
17	M	38	2	No	GTR	GBM	Right frontal	50	50
18	M	66	3	Yes	GTR[c]	GBM	Left multicentric	60	40
19	M	55	2	No	GTR	GBM	Left frontal	60	70
20	F	54	2	No	GTR	GBM	Right parietal	60	80
21	F	77	2	Yes	GTR[c]	AA	Left multicentric	80	90
22	F	38	2	No	GTR	GBM	Left frontal	50	50
23	M	75	2	No	GTR	GBM	Right frontoinsular	80	80
24	M	55	2	No	GTR	AO	Right rolandic	70	70
25	M	63	2	Yes	GTR	AO	Right frontal	60	60
Mean		57.96						66.80	69.20

[a]i-CT, intraoperative computed tomography; KPS, Karnofsky Performance Status; F, female; GTR, gross total resection; GBM, glioblastoma multiforme; M, male; AA, anaplastic astrocytoma; AO, anaplastic oligodendroglioma.
[b]According to intraoperative findings, as reported in operating theater medical records.
[c]GTR for multicentric tumor is intended as complete resection of the larger tumor together with separate nodules.

In 6 of 8 cases, we were able to see peripheral vague fluorescence around the edges of residual tumor (confirmed by neuronavigation). In such cases, the resection was extended to include those infiltrating areas. Revision surgery for residual tumor was never required. Only 1 patient in Group A experienced a postoperative hemorrhage that required a second surgery. Major complications were not observed

in either group. One patient in Group B experienced a transient worsening of preoperative neurological conditions; however, these completely recovered before discharge.

EOTR Analysis

In Group A patients (excluding the case of intended biopsy), the preoperative mean volume was 30. 90 cm3; residual disease was found on 7 early postoperative MRI examinations, with a mean volume of 1.16 cm3.

In Group B, the preoperative mean volume was 36.90 cm3; residual tumor was found in 6 patients, with mean volume of 0.628 cm3.

With regard to Group A, patients with residual disease showed a mean 97.3% EOTR; in Group B, the mean resection rate was 98%.

The Student t test did not show any statistically significant difference in EOTR, measured by volumetric MRI, in the 2 groups (P = .5). Table 2 summarizes the results of the EOTR analysis (

Table 2).

TABLE 2. Extent of Tumor Resection Analysis in Both Groups

	Group A	Group B
Mean preoperative volume, cm^3	30.90	36.90
Range	0.8-84.3	8.0-85.4
SD	24.66	22.97
2-Dimensional maximal length, mm	45.65	51.0
Range	11.0-75.0	30.0-75.0
SD	17.40	13.43
Mean short axis, mm	31.76	32.0
Range	9.0-49.0	21.0-47.0
SD	11.76	7.27
Residual disease volume, cm^3	1.16 (7 cases)	0.628 (6 cases)
Range	0.12-2.20	0.16-1.67
Extent of tumor resection, %	97.3	98.0
Range	96-98.6	93.5-99.7

The Student t test did not document statistically significant differences in age and sex distribution of both groups (P = .06 and .08, respectively). The KPS score changed from a preoperative mean of 67 to 69 after surgery in Group A and from a mean of 74 to 77 in Group B, respectively. Comparison of postoperative KPS score in both groups, verified by the application of the Student t test, did not show statistically significant differences (P = .07).

Groups A and B did not show differences in OS and PFS: P = .61 and .46, respectively, by the log-rank test (Figure 1).

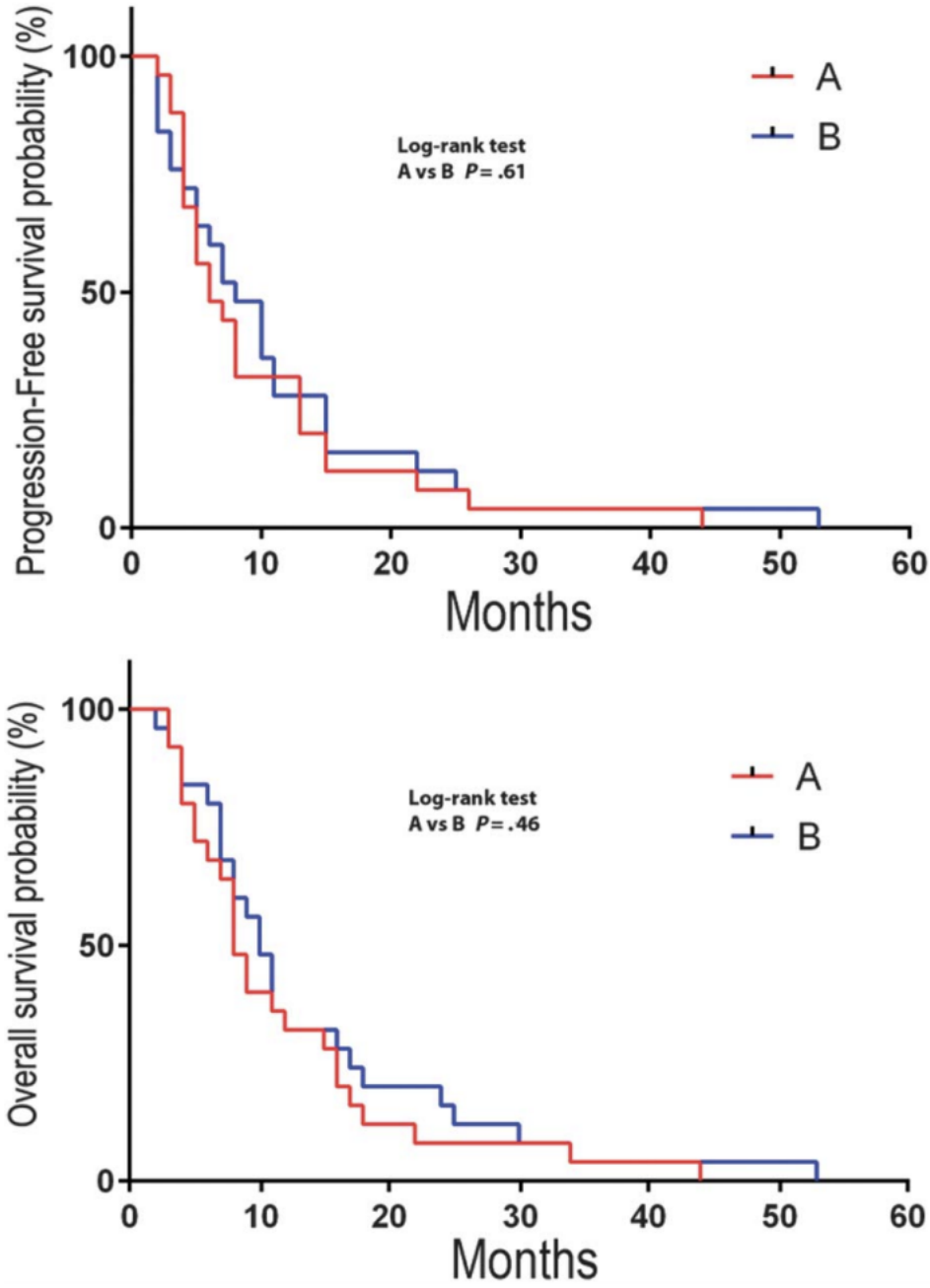

Figure 1: Overall survival and progression-free survival according to the Kaplan-Meier method in group A and B patients showing no statistically significant difference.

4. Prospective clinical study on intraoperative imaging-guidance

4.1 Methods

50 patients (27 males), with a mean age of 63.8 years (range 49-82), suffering from radiologically suspected HGG (i.e. with evocative MR-spectroscopy) were prospectively enrolled and followed-up from June 2015. Patients with recurrent tumors, previous tumor biopsy or partial resections were not considered for inclusion. Paediatric patients as well as those with multifocal disease on MRI were also excluded. In all patients included, a complete resection of enhancing tumor was deemed feasible preoperatively. Radiological diagnosis was confirmed by histology in all cases; in cases with pathological findings not compatible with glioblastoma patients were subsequently excluded. Our standard MR protocol included volumetric T1-weighted, without and with gadolinium enhancement, and volumetric FLAIR sequences as well as T2-,, DWI- and, MR-spectroscopy images. In 38 of 48 patients MR-DTI sequences were also acquired and 3D tractography was obtained to study pre- and intra-operatively anatomical relationship between tumors and white matter eloquent fibers. All exams were performed using the same MR machine (Philips 1.5T MRI systems) by three different neuroradiologists with proven experience in brain tumors. Volumetric evaluation of pre-operative MR was performed both on gadolinium-enhanced T1-weighted 3D sequences and FLAIR 3D sequences. Volumetric reconstruction and measurement was carried out using a manual segmentation method. StealthViz® (Medtronic Inc. - USA) software was used for segmentation, 3D rendering and reconstruction as well as for volumetric measurements. On gadolinium-enhanced T1-weighted images, all slices showing pathological contrast enhancement were segmented and reconstructed. On FLAIR images segmentation was based on the differences in signal intensity found in the peritumoral areas. As known (24), the brain area surrounding the contrast-enhancing tumor has a higher signal intensity compared to the more distant white matter, showing a FLAIR signal similar to oedema observed in non-infiltrating tumors (i.e. meningioma, metastases). The edges of different peritumoral areas, with different signal intensity, were determined by placing some regions of interest (ROIs) in the hyperintense brain surrounding the lesion. This method allowed to estabilish a threshold to distinguish areas of "true" tumor infiltration from areas of oedema/brain reaction. Based on such threshold, manual segmentation of the tumor, including peri-tumoral infiltrative areas, was performed on 3D FLAIR images. Consequently, for each patient a double volumetric evaluation was performed on pre-operative MR. Both 3D T1 and 3D FLAIR sequences, after segmentation and rendering, were made available for neuronavigation. All patients included underwent 5-ALA fluorescence guided resection. 1,5 grams of 5-ALA hydrochloride (5-ALA HCL, Gliolan, Medac GmbH - Germany) were administered 3 hours before anaesthesia to the patient. An ultraviolet filter integrated in the microscope lamp (OPMI Pentero – Zeiss - Germany) was used to stimulate fluorophores making visible the fluorescent tissues.

The StealthStation S7® (Medtronic Inc. - USA) navigation system was used in all cases. Gadolinium-enhanced, T1-weighted, 3D sequences and FLAIR 3D sequences were used for intraoperative navigation. The two datasets were merged before patients′ registration using the software provided by the navigation system. T1-sequences were used as reference exams and optic or electromagnetic skin tracer was used for patients′ registration. During microsurgery, continuous neuronavigation was performed, using the focus of the microscope (OPMI Pentero – Zeiss - Germany) as navigation pointer. Microsurgical videos (obtained alternating white and ultraviolet light) were also visualized on navigation system screen to obtain immediate comparison between MR images (Gad-T1 and FLAIR) and intraoperative findings. When resection of the enhancing tumor was deemed complete, according to Gad-T1 navigation data, all residual white matter areas still showing fluorescence were identified and localized with navigation. A comparison between abnormal areas based on gadolinium-enhancing T1 and FLAIR signal was then performed.
All patients underwent post-operative MR within 48 hours after surgery. Post-operative MR protocol included volumetric T1-weighted, without and with gadolinium enhancement, and volumetric FLAIR sequences as well as T2- and DWI-weighted images. Hyperintense areas in the context of surgical cavity, visualized on T1 sequences before and after gadolinium administration, were interpreted as blood clots and not considered for the extent of tumor resection (EOTR) analysis. Volumetric measurement of residual tumor was made using the same method above described for pre-operative assessment on gadolinium-enhanced, T1-weighted and FLAIR images (Figure 2). EOTR analysis was then performed by calculating the rate of tumor resection, considering the values of pre- and post-operative tumor volumes on gadolinium-enhanced, T1-weighted and FLAIR sequences, according to the following formula (SANAI BERGER): [(preoperative tumor volume – postoperative tumor volume) / preoperative tumor volume] x100 (16).

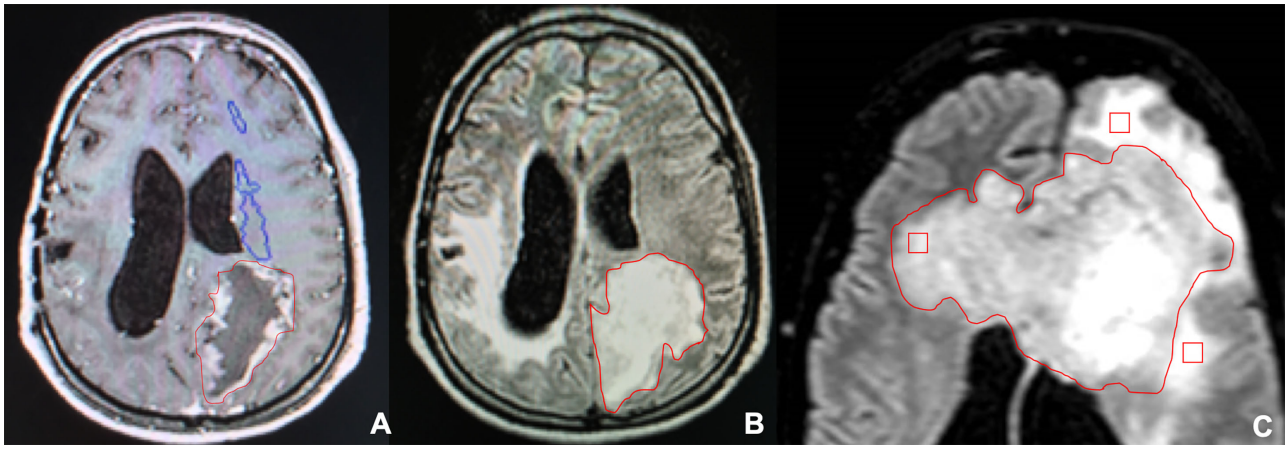

Figure 2: Manual segmentation based on T1-Gad (A) and FLAIR (B) sequences for volumetric evaluation of HGG. The segmented pathological area on FLAIR sequences was selected according to the hyperintensity value recorded by multiple ROIs placed in different peritumoral areas, in each

slice used for segmenation (C). In this case the yellow ROI revealed a lower hyperintensity value than two red ROIs periferically placed. This allows to differentiate tumor (yellow ROI), included in segmented areas, from edema (red ROIs) excluded from segmented lesion.

Overall Survival (OS) and Progression Free Survival (PFS) was recorded for each patient included in the study. For surviving patients who are still undergoing clinical and radiological follow-up every three months, survival data were calculated at last follow-up visit in January 2018. Tumor progression was defined according to the Response Assessment in Neuro-Oncology Criteria (RANO Criteria) (25), based on a scheduled follow-up scheme including brain MR performed every three months. Positron Emission Tomography with 11-C L-Methionine (11CMet-PET) was also used to differentiate real tumor progression from radionecrosis or pseudoprogression. Karnofsky Performance Score (KPS) was used to assess patients′ clinical status pre- and postoperatively and during follow-up.
Statistical analysis was performed using the SPSS 22.0 software (IBM, New York - USA). Student T-test was used to verify the presence of statistically significant differences between pre-operative tumor volumes measured on T1 and FLAIR sequences. Linear regression analysis investigated the statistical correlation between survival and radiological data obtained from volumetric measurements and EOTR assessment.

4.2 Results

Patients included in the present study did not experience major and minor complications related to surgery. We did not observe any death in the early post-operative period nor within the first month after surgery. All patients underwent the same post-operative adjuvant treatment, based on Stupp protocol. Radiotherapy with concomitant oral temozolomide was started within 50 days after surgery.
Histologic examination revealed glioblastoma (G IV according to WHO) in 44/50 cases, gliosarcoma (GIV WHO) in 3/50 and anaplastic astrocytoma in 3/50.
Mean pre-operative tumor volume on gadolinium-enhanced, T1-weighted MR sequences was 54.9 cc (range 33.4cc - 89.7cc), whereas mean pre-operative tumor volume on FLAIR sequences was 72. 6 cc (range 39.5cc – 103.8 cc). Paired student T-test revealed statistically significant differences between the two series of data ($p<0.05$). Tumor volumes calculated on contrast-enhanced T1-weighted images were constantly smaller than those obtained from 3D FLAIR-weighted sequences.

KPS changed form a mean pre-operative value of 75.4 to a mean post-operative value of 64.8. The KPS registered at last follow-up control was 76.6. No statistically significant differences in KPS variations were documented during follow-up (range 12-36 months).

Neurological worsening related to surgery was documented in 6/50 patients (12%). Three of these six patients suffered from permanent neurological deficits, whilst in the other three patients neurological impairment was transient and recovered within 3 months after surgery. In all cases experiencing post-operative neurological worsening, intraoperative neuromonitoring (cortical and subcortical electrical stimulation as well as MEPs and SSEPs recording) had been used.

In all patients, fluorescent areas were entirely resected if neuromonitoring ruled out the presence of eloquent tissue. Evidence of fluorescent tissue beyond the contrast-enhancing edges of the tumor, according to neuronavigation data, was documented in 47/50 patients (94 %). Interestingly, in such cases neuronavigation based on 3D FLAIR images revealed a constant correspondence between 5-ALA fluorescent and hyperintense areas, pre-operatively segmented as tumor and not oedema.

Volumetric evaluation of EOTR based on gadolinium-enhanced, T1-weighted sequences documented residual tumor in 3/50 (6%) patients. Mean residual tumor volume was 1.76cc (range 0 .9cc- 1.8cc). Conversely, EOTR evaluation based on FLAIR sequences revealed residual tumor in 33/50 (66%) patients. Mean residual tumor volume measured on 3D FLAIR images was 3.7cc (range 0.4 cc – 8.7 cc). The mean EOTR rate calculated on the two different imaging modalities (gadolinium-enhanced, T1-weighted and FLAIR MR sequences) resulted 99.8% (range 95.6%-100%) and 93.45% (range 70.4%-100 %), respectively. Comparison of such data revealed statistically significant differences in post-operative residual tumor volumes according to the paired Student T-test ($p<0.05$).

Mean OS and PFS were, respectively, 23.12 months and 18.72 months. 9/50 patients (18%) are still alive and under follow-up.

Linear regression analysis (Figure 3) revealed positive correlation between PFS and FLAIR-based EOTR rate (R2=0.41) as well as between OS and FLAIR-based EOTR rate (R2=0.59). Weak correlations were found relating PFS and OS to gadolinium-enhanced, T1-weighted-based EOTR (R2=0.028 and 0.006, respectively). A stronger correlation was also found between residual tumor volume measured on FLAIR rather than on gadolinium-enhanced, T1-weighted MR images and overall survival (R2=0.28 and 0.007, respectively).

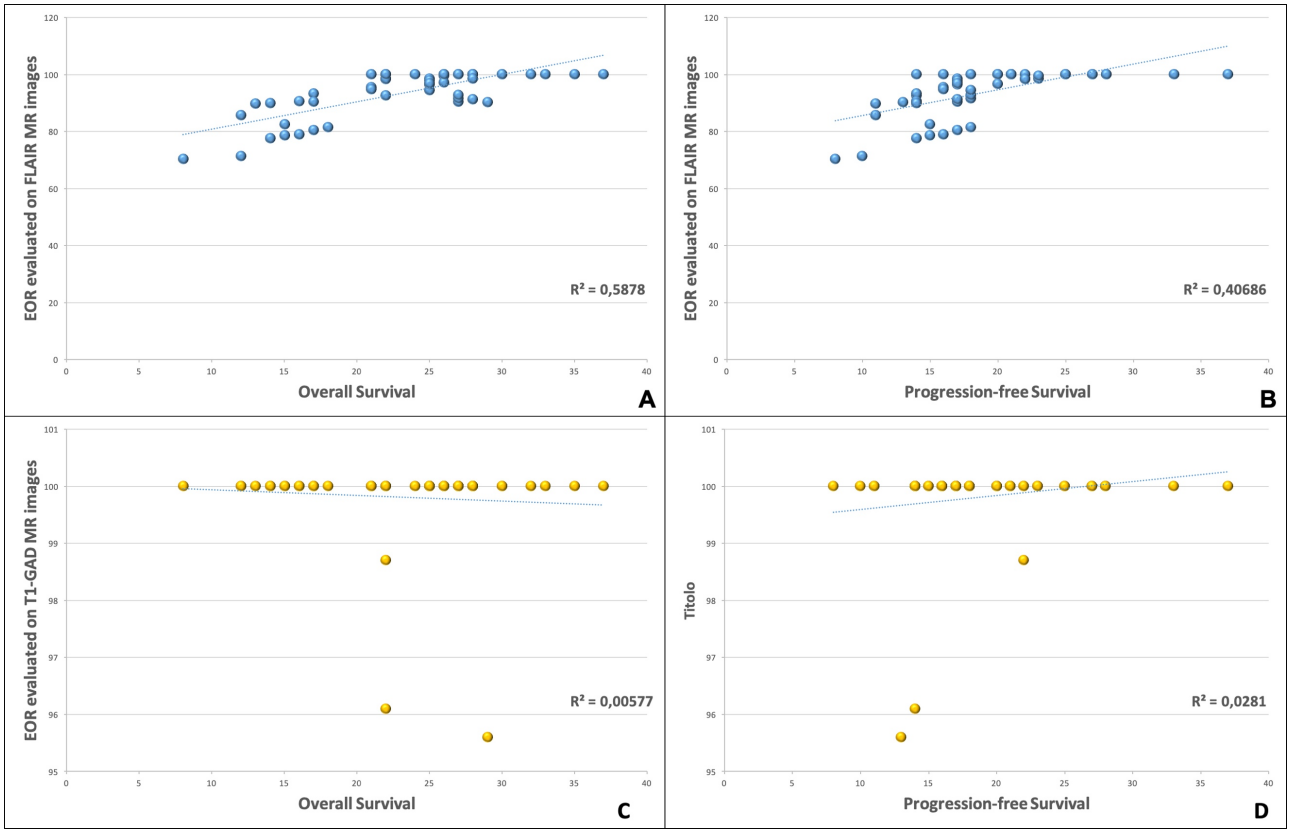

Figure 3: Linear regression analysis demonstrated the presence of a positive correlation between FLAIR-based Extent of tumor resection values and Overall Survival (A), and Progression Free survival (B). No significant correlation between survival parameters and T1-Gad-based Extent of resection evaluation was documented (C, D).

5. In vitro experiments on temozolomide

5.1 Methods

5.1.1 Preparation of TMZ-loaded nanoparticles

The preparation of the temozolomide encapsulated in nanoparticles has already been described in the literature. Temozolomide (TMZ) has been purchased by Merck & Co., Inc. (Whitehouse Station , NJ, USA). Different nanoparticles have been synthetized at Department of "Scienze del Farmaco" University of Catania whereas nanoparticles combined with monoclonal antibodies have been obtained at Department of "Biologia e Biotecnologie - Charles Darwin" Sapienza University, Rome .

In our experiments, we started investigating two different nanocarriers: poly lactic-co-glycolic acid (PLGA) and chitosane. Both nanosystems were combined with temozolomide, and investigated "in vitro".

Only the nanosystem created by the combination of PLGA with TMZ has been selected for in vivo experiments, for several reasons.

The encapsulation of TMZ in PLGA NPs has been already demonstrated as a suitable strategy to increase TMZ therapeutic efficacy and to overcome its limitations, as toxicity in healthy tissues by targeting the tumour cells. Also, TMZ encapsulation in PLGA NPs should enhance drug transport across the BBB and avoid drug recognition by p-glycoprotein pump in target cells circumventing drug efflux. Moreover, these NPs exhibit low synthesis complexity (26) and are able to maintain a controlled drug release for several days, decreasing the need for frequent drug administration and doses, minimizing the side effects in healthy tissues (27). The PLGA polymer can also be easily functionalized for the design of NPs with different targeting
moieties (28).

The steps of preparation of TMZ-loaded in PLGA-PEG nanoparticles included:

- PLGA, PEG and TMZ were dissolved in a solvent (ACETONE).
- TMZ (3 mg) and PLGA-PEG-FOL copolymer (30 mg) are dissolved in DMSO (3 mL) and the DMSO solution is added dropwise (0.3 mL/min)
- Stirring for 2 hrs to allow diffusion of the organic solvent.
- The resulting solution has been centrifuged at 25,000 rpm for 30 min and the nanoparticles that appeared as the pellet were subjected to freeze-drying.
- The lyophilised nanoparticles were weighed and dissolved in acetonitrile, and the amount of encapsulated TMZ was determined by UV/Vis spectrophotometry

The steps of preparation of TMZ loaded in Chitosane nanoparticles

- Chitosane and TMZ were dissolved in a solvent (ACETONE).

- TMZ (3 mg) and chitosane (30 mg) are dissolved in DMSO (3 mL) and the DMSO solution is added dropwise (0.3 mL/min)
- Stirring for 2 hrs to allow diffusion of the organic solvent.
- The resulting solution has been centrifuged at 25,000 rpm for 30 min and the nanoparticles that appeared as the pellet were subjected to freeze-drying.
- The lyophilised nanoparticles were weighted and dissolved in acetonitrile, and the amount of encapsulated TMZ was determined by UV/Vis spectrophotometry

5.1.2 Cell lines

Primary cell lines of glioblastoma U251 and U87 have been obtained from laboratories of Department of "Scienze Biomediche e Biotecnologiche - Biometech" University of Catania used, both derived from human glioblastoma and commonly used in pre-clinical studies on glioblastoma. The cytotoxicity towards these cell lines of the two nanopharmaceuticals obtained will be measured and compared with the temozolomide in standard formulation (free). All the used lines were cultured in high-glucose Dulbecco's Modified Eagle medium (DMEM), supplemented with 10% fetal bovine serum (FBS) and 1% penicillin-streptomycin. Cells were maintained at 37 °C in a humidified 5% CO2 incubator. At 80% of confluence, the cells were trypsinized and subcultured. Both U251 and U87 cell lines were chosen since they show significant similarities with the genetic, immunohistochemical and histological and characteristics of human GBM tumor (29).

5.1.3 Preparation of TMZ-loaded mAb-PLGA NPs

TMZ-loaded PEG-PLGA NPs were prepared using also the single emulsion-solvent evaporation technique. 8 mg of non-modified PLGA was added to the previously prepared PEG-PLGA. Also 1 mg TMZ was added to the PLGA mixture in dichloromethane, and the remaining protocol was performed as described previously in section 5.1.2. The prepared NPs were next modified with OX26 mAb by a covalent coupling reaction at a molecular ratio of OX26 mAb: PEG-PLGA of 1:2. The maleimide group on PEG extremity reacts with thiol groups present on mAbs, after mAb activation by Traut′s reagent. A drop of EDTA was added to prevent oxidation of the thiol groups (30). The activated mAbs were separated from the excess reagents by size exclusion chromatography (PD Minitrap G-25 columns containing Sphadex Medium, GE Healthcare, Sweden). The activated mAbs were then added to the previously prepared PEG-PLGA NPs and incubated 1 h in the dark at RT, followed by overnight incubation at 4 °C. Non-attached antibody was removed by centrifugation (30 min, 14100 g).

5.1.4 PLGA NPs physicochemical characterization

The physicochemical features of the prepared NPs, as mean diameter, size distribution and zeta potential values, were assessed by Dynamic Light Scattering (DLS) and by laser doppler velocimetry methods. The measurements were performed in a ZetaSizer Nano ZS, Malvern Instruments, UK. The average NP size was obtained by measuring the fluctuations of scattered light intensity as a function of time. These fluctuations can be related to the NPs diffusion coefficient and size, using the Stokes-Einstein Equation. The attained data is given in intensity distribution. The zeta potential data analysis was performed using the dielectric constant of water and the zeta potential values were estimated by Smoluchowski approximation from the electrophoretic mobility. The morphological analysis of the NPs was obtained by Transmission Electron Microscopy (TEM). The samples were visualized on copper grids (Formvar/Carbon-400 mesh Copper, Agar Scientific, UK) and negatively stained with a 2% (v/v) uranyl acetate solution.

5.1.5 TMZ encapsulation efficiency and release from PLGA NPs

The TMZ encapsulation efficiency (EE) and its release from PLGA NPs were determined by UV−Vis spectrophotometry at λmax 265 nm. Free TMZ was obtained from centrifugation of NPs suspension (30 min, 14100 g), and quantified using a calibration curve of known TMZ concentrations (UV-1700 PharmaSpec, Shimadzu, Japan). The TMZ loading capacity of the prepared PLGA NPs was also determined by the following equation: (amount of encapsulated TMZ/polymer weight x 100).

In vitro temozolomide release studies were performed, over 20 days at 37° C, using a cellulose dialysis membrane diffusion technique. A sufficient amount of TMZ-loaded PLGA NPs was diluted in 2 mL of release buffer (PBS, pH 7.4, 0.01 M) and placed into a dialysis device (Float-A-Lyzer G2, CE, 10KDa, SpectrumLabs (Laguna Hills, CA)). The outside space of the dialysis device was filled with 4 mL of release buffer. At predetermined times, samples were collected from the outside medium and, after measurement by UV-Vis spectrophotometry, returned to the release medium. A solution of TMZ in PBS was used as control.

5.1.6 Cellular imaging studies

The NPs in vitro uptake in the human cells lines (U251, U87) was assessed using laser scanning confocal microscopy (LSCM) (Leica TCS SP5 II, Leica Microsystems, Germany). For that purpose, C6-loaded NPs were used. This fluorescent marker is distributed in the NPs matrix, allowing the visualization of the NPs inside the cellular compartments (31). 1000 cells/well were seeded in 12-

well plates (Ibidi, Germany) and allowed to attach for 24 h (37 °C, in a humidified 5% CO2 incubator). Cells were then treated with mAb modified and unmodified C6-loaded NPs for 2 and 72 h. After the incubation period and subsequent wash with PBS, the cells were fixed with 4% (w/v) paraformaldehyde. The acidic cell compartments (as endosomes/lysosomes) were stained with LysoTracker® Red and cell nuclei were marked with DAPI. At least six images from different areas of each cell lines were acquired in emission mode. Untreated cells were also used control.

5.1.7 Quantification of in vitro cellular uptake of mAb-PLGA NPs

Cellular uptake of mAb-modified and unmodified PLGA NPs was quantified by a fluorescence assay using C6 loaded PLGA NPs. U251 and U87 cells were seeded in 96-well plates at a density of 8000 cells per well and allowed to attach for 24 h. Six NPs samples were diluted in cell culture medium at final polymer concentration of 50 μg/mL, and the cells were incubated with these samples for 0.5 h and 2 h. At the end of the incubation period, the cells were washed with cold PBS to remove the non-internalized NPs. The cells were then lysed with 0.1% Triton X-100 in 0.1 N NaOH solution. The fluorescence intensity from C6-loaded NPs was measured using a fluorescence microplate reader (HT Microplate Spectrophotometer, BioTek) with excitation and emission wavelengths set at 430 and 485 nm, respectively.

5.1.8 Transferrin competitive binding assay

Transferrin blocking assay was used to confirm whether the mAb-PLGA NPs are internalized through transferrin receptor-mediated endocytosis. Competitive binding to TfRs was achieved using an excess of transferrin, and cellular uptake of PLGA NPs was quantified by fluorescence using C6 as mentioned above. U251, U87 and NHA cells were seeded in 96- well plates at a density of 8000 cells per well and allowed to attach for 24 h. Transferrin was diluted in cell culture medium and added to the cells at six final different concentrations ranging from 1 to 10 mg/mL. The same range of concentrations of folate was used as control. After 1 h, cells were incubated for 2 h with C6-NPs samples at final polymer concentration of 50 μg/mL.

At the end of the incubation period, the cells were washed and lysed as described in the previous section. The fluorescence intensity from C6-loaded NPs was measured with excitation and emission wavelengths set at 430 and 485 nm, respectively.

5.2 Results

5.2.1 PLGA NPs physicochemical properties

Different TMZ-loaded nanoparticles were prepared during our experiments. In all the prepared formulations based on PLGA, PVA was used as an emulsion stabilizer since it has a high affinity to PLGA and forms a uniform layer on the NPs′ surface, conferring stability against aggregation (32). Maleimide-functionalized PEG was also used to allow covalent coupling of OX26 mAb at the PEG terminus with the chemically reactive end-group. The physicochemical properties of the prepared NPs were evaluated and are presented in Table 3.

PLGA Nps	Mean size (nm)	PdI	Zeta Potential (mV)
Unloaded PLGA NPs	176 ± 3	0.086 ± 0.015	- 29 ± 3
TMZ-PLGA NPs	181 ± 2	0.059 ± 0.012	- 25 ± 4
mAb-PLGA NPs	193 ± 4	0.067 ± 0.018	- 30 ± 1
TMZ-mAb-PLGA NPs	194 ± 1	0.074 ± 0.024	- 20 ± 2

Table 3: Physicochemical features of different Nanoparticles

The prepared unloaded NPs exhibited a mean diameter of 176 ± 3 nm, and a zeta potential value of -29 ± 3 mV, negative as expected due to the negative charge of the carboxylic groups of PLGA polymer (Table 1). The TMZ molecules accommodation in the polymeric matrix caused a significant ($p<0.05$) increase in size for the TMZ-PLGA NPs (181 ± 2 nm).
Moreover, NPs mean size was also significantly increased with OX26 mAb modification (194 ± 1 nm) ($p<0.05$), indicating an efficient conjugation since the diameter of the globular antibody is

approximately 15 nm (33). The prepared nanocarriers exhibited a small size distribution (PdI ≤ 0.1). Loading of the NPs with TMZ did not significantly affect their zeta potential, however a small decrease was observed due to the adsorption of TMZ molecules on PLGA NPs surface, exerting a masking effect on the superficial net charge (34). The modification of the NPs′ surface with mAb also does not significantly alter their zeta potential, due to the negative nature of this immunoglobulin ($p>0.05$). The colloidal stability of the prepared NPs is a result of electric charge of the carboxylic groups at the NP surfaces, and the PVA layer on the NP′s surface causing steric repulsions. In fact, TEM demonstrates a stabilizer layer surrounding PLGA NPs. TEM also shows uniform PLGA NPs with a spherical form. The mean size of the NPs revealed by TEM are in agreement with those determined by DLS analysis. NP dimensions and zeta potential are key parameters that affect the efficiency of NP systemic circulation, and uptake by target cells (35). Also transport across the BBB will depend on these parameters. Although mAb modification of the NPs′ surface is expected to enhance the transport of NPs across the BBB through receptor-mediated transport, these two physiochemical characteristics also are determining factors. Thus, these parameters were considered during the design of this nanosystem. The prepared mAb-modified PLGA NPs exhibit suitable physicochemical characteristics for cancer cell uptake and transport across themBBB. Since neutral and anionic NPs are more easily transported across the BBB and are not associated to BBB toxicity (36), most of the NP formulations described in the literature for brain delivery have moderate to high (between −1 to −45 mV) negative zeta potentials, as the one prepared in this work (37). It has also been proven that NPs with dimensions up to 200 nm are more easily accumulated in brain tissue (38) since tumor microenvironment exhibits vascular fenestrations in the range of 40−200 nm (36). Also, NPs with dimensions up to 200 nm are more efficiently taken up by receptor-mediated endocytosis, as it was intended in this work with the use of TfR (39).

The stability of the prepared NPs was assessed in terms of size and zeta potential, and no changes were observed (data not shown), proving that the developed system is stable at storage conditions (4 ºC), for at least one month. The binding ability of the mAb-modified NPs to TfR was evaluated by ELISA assays.

OX26 mAb-modified NPs showed significantly higher absorbance at 405 nm (0.81 ± 0.05) than non -modified NPs (0.29 ± 0.08) ($p<0.05$). Therefore, OX26 mAb demonstrated that the bioactivity for the TfR is preserved after the mAb conjugation with the NPs.

5.2.2 TMZ encapsulation efficiency and release from PLGA NPs

PLGA NPs loaded with TMZ showed encapsulation efficiencies ranging from 48 ± 10% for mAb-PLGA NPs to 44 ± 3% for non-modified NPs, respectively. Drug loading varied from 10 ± 2% for mAb-PLGA NPs to 9 ± 1% of the polymer weight for non-modified NPs. These NPs were subsequently evaluated for their ability to sustain the release of TMZ for cancer cell therapy. The in vitro release profile of TMZ from PLGA NPs was evaluated at 37 °C in PBS (pH 7.4, 0.01 M) to mimic the physiological pH and salt concentrations.

The TMZ release can be justified by two possible mechanisms. In aqueous medium, the esters bonds of PLGA are hydrolyzed causing the erosion of the polymeric matrix, allowing the release of the entrapped TMZ molecules. TMZ is also released by diffusion through the polymeric matrix. Thus, the release rate of a drug will depend upon different factors such as drug physicochemical properties and geometry of drug-loaded PLGA NPs (size and shape) (39).

The dialysis method was used to compare the release of encapsulated TMZ with free TMZ. TMZ molecules were released in a biphasic release pattern, composed of an initial rapid released followed by a slower and controlled release, characteristic of PLGA NPs. As Figure 2 shows, 36± 6% of the total TMZ was released at the first 24 h for mAb-modified PLGA NPs and 43 ± 1% for non-modified NPs, respectively. When in aqueous medium, the surfaceadsorbed TMZ molecules are rapidly released from the NPs, explaining the verified burst release. The TMZ entrapped in NPs polymeric matrix exhibited a slower and controlled release for several days. The conjugation of mAbs on the surface of the PLGA NPs affected the TMZ release from the PLGA NPs, since it was observed a higher release from non-modified PLGA in comparison to mAb-PLGA NPs. Non-modified PLGA NPs exhibited a total release of TMZ (98 ± 2%) after 9 days, while mAb-modified NPs only released about 78 ± 2% of entrapped TMZ at day 20 (Figure 4). These results may be explained by the mAb molecules linked to the surface of the NPs that may obstruct water permeation, hindering the diffusion of the drug molecules as previously reported (30).

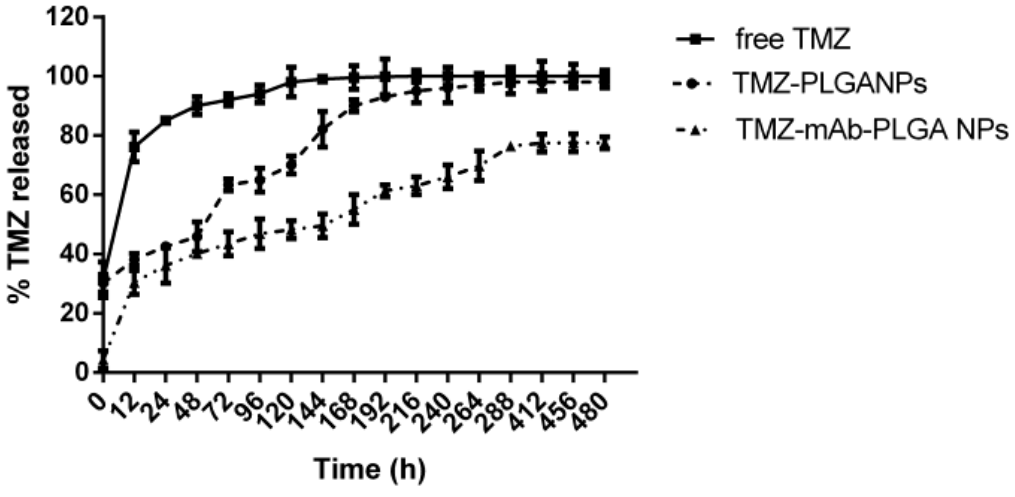

Figure 4: In vitro temozolomide release studies were performed, over 20 days at 37° C, using a cellulose dialysis membrane diffusion technique.

5.2.3 Cell viability test

In the first step of the study U87 viability have been tested, using the first two compounds initially synthetized (Chitosane NPs and PLGA-PEG NPs): results are summarized in the following figures (Figures 5, 6)

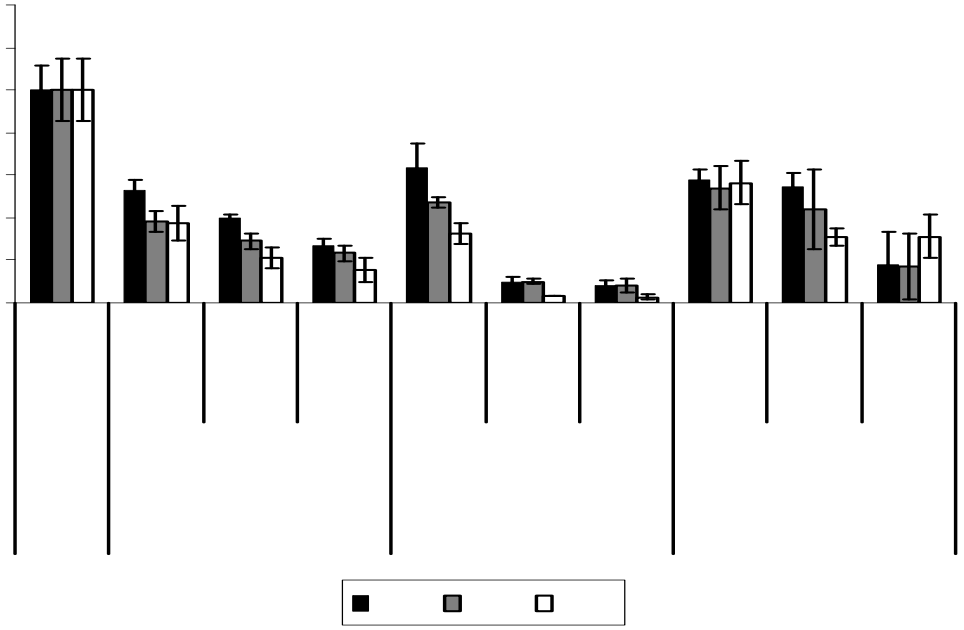

Figure 5: Cell viability at three times intervals of two different nanosystems at different concentration compared with free Temozolomide. For NPs, the reported concentrations refer to quantity of TMZ that has been efficiently loaded into nanoparticles. Each result was compared to untreated cells (control).

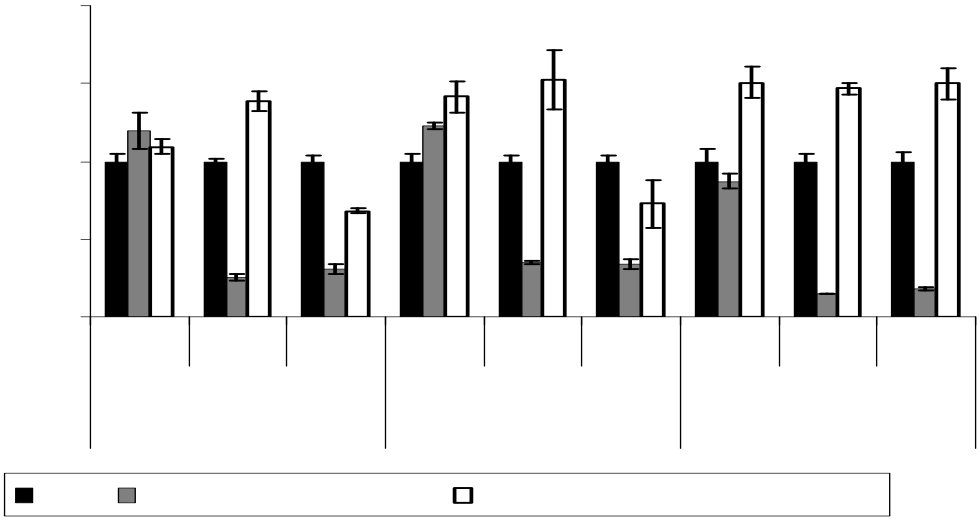

Figure 6: Cell viability at three times intervals of two different nanosystems at different concentration compared with free Temozolomide. For NPs, the reported concentrations refer to quantity of TMZ that has been efficiently loaded into nanoparticles. Each result was compared to cell treatments with TMZ at same concentration and time of incubation.

5.2.4 In vitro cellular uptake of mAb-PLGA NPs

Coumarin-6 was used as fluorescence marker to visualize the cellular uptake of the prepared PLGA NPs by confocal microscopy, in malignant glioma cell lines, U87 and U251. This fluorescent dye is distributed in the NPsmatrix, allowing their visualization inside the cellular compartments since during the time of the experiment only about 13% of the dye is released from the NPs (data not shown). The cell nuclei were stained with DAPI and the acidic compartments, as endosomes and lysosomes, with LysoTracker Deep Red. The confocal images of non-treated and mAb-C6-PLGA NPs treated cells are presented in Figure 7.

The colocalization of PLGA NPs within the late endosomes/lysosomes is represented by the yellow/orange color. Scale bar: 25 μm. After 2 h incubation, the NPs were uptaken by all the treated cells. The colocalization of C6-NPs and lysotracker-stained lysosomes is represented by the yellow/orange dots, due to the combined fluorescence of green and red emission, respectively (40), suggesting that the NPs are internalized by an endocytic mechanism (Figures 7B and 7E). Also, as shown in Figures 7C and 7F, after 72 h incubation it is possible to visualize the NPs in the cytoplasm, suggesting that the NPs can escape the endo-lysosomal compartments. The images

after 72 h incubation also show a decrease in the number of cells, due to the antiproliferative activity of the TMZ entrapped in the NPs. All the attained results suggest that these mAb-PLGA NPs, being internalized by endocytosis mechanism, are able to efficiently perform as cytoplasmic drug delivery vehicles, avoiding multidrug resistance mechanisms such as TMZ efflux from target cells.

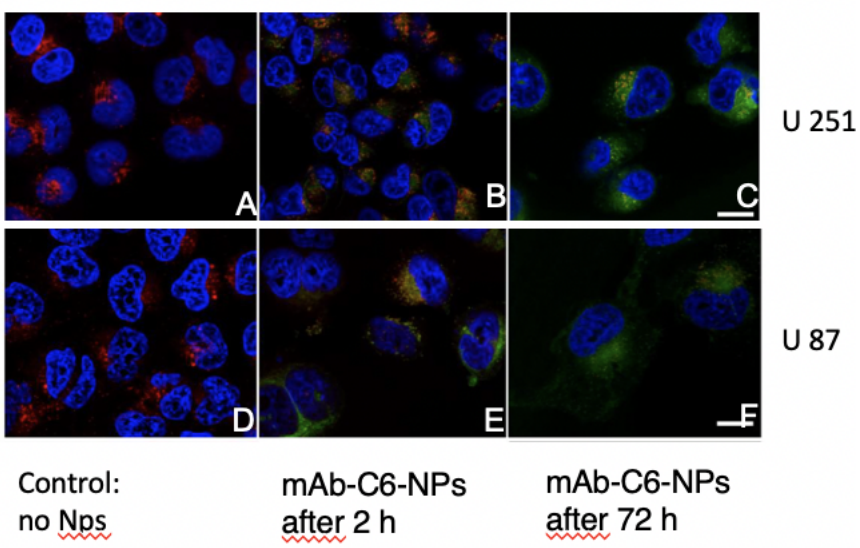

Figure 7: Confocal microscopy. Coumarin-6 was used as fluorescence marker: nuclei are marked in blue, the acidic compartments (late endosomes/lysosomes) in red and the mAb-C6-NPs in green.

5.2.5 Selective cellular uptake of mAb-PLGA NPs

C-6 was also used to quantify the cellular internalization of the PLGA NPs in U251 and U87 cell lines. The cellular internalization of mAb-modified and non-modified PLGA NPs was measured after 0.5 and 2 h of incubation, respectively.

As the attained results show, the NPs were efficiently internalized by the cells, showing that the longer the incubation time, the higher the cellular uptake ($p<0.05$). Also, modification of the PLGA NPs surface with mAb for Transferrin Receptor (TfR) significantly increased the cellular internalization in all the studied cell lines for 2 h incubation period ($p<0.05$). Cellular uptake of mAb-NPs by U251 cells after 0.5 h and 2 h of incubation was found to be 1.89 and 1.37-fold higher than unmodified NPs, respectively. For U87 cells, the cellular uptake for mAb-NPs was 1.70 and 1. 41-fold higher in 0.5 and 2 h incubation, respectively.

Tf competitive binding assay was used to investigate how TfR impacts the mAb-PLGA NPs cell internalization. Cells were pre-treated with increasing doses of Tf to block the TfR before the

incubation with NPs. As Figure 4D shows, cellular internalization of mAb-NPs significantly decreased with blockage of TfR in a dose-depend manner, in all the studied cell lines ($p<0.05$). It was observed a decrease between 43 and 48% in the internalization of mAb-NPs when using 10 mg/mL of Tf. Blockage of the TfR did not affect the internalization of the non-modified NPs. The same blocking experiment, using folate instead of TfR, was used as control, showing that pretreatment with folate did not exhibit any effects on the mAb-NPs uptake. Confocal studies displaying NPs in late endosomes/lysosomes suggest that these NPs are selectively uptaken by TfR-mediated endocytosis.

6. In vivo experiments on temozolomide

6.1 Methods

6.1.1 Model of glioma-bearing rats

Ten male Sprague-Dawley rats (weighing 180−220 g) were maintained at 22° C on a 12-h light/dark cycle in polyethylene cages with ad libitum access to food and water. GBM development was induced by intracranial implantation of C6 cells.

Rats were anesthetized by intraperitoneal (i.p.) injection of 10% chloral hydrate (0.4 mL/kg), and then C6 cells (1x106 cells in 6 lL of DMEM) were injected stereotactically into the right caudate nucleus (3mm lateral to the bregma and 5mm deep from the dura) using a microsyringe (Hua et al., 2018). The wounds were closed with sutures and sterilized with iodophor. Antibiotic drug was injected intramuscularly, and the rats were carefully monitored until recovery from anesthesia. After implant, the animals provided with free access to standard chow pellets, water and were housed in colony cages with the environmentally controlled conditions. The animals were divided into 5 groups consisting of 2 animals and formulations were administered gently in rats′ nostril to inhale the each formulations.

The formulations were delicately administred (in order to avoid mucosal damages) using 2cm polyethylene tube attached to micro syringe.

6.1.2 In vivo brain distribution of NPs

The brain hemispheres collected after sacrificing rats were washed and dissected. The brains were homogenized by adding methanol and stored at -20°C until use. The sample was mixed with internal standard, i.e., caffeine (500 ng/mL), and acetonitrile (2mL) was added to precipitate the protein. 2mL diethyl ether added to above sample to extract the TMZ and then centrifuged at 4000 rpm for 5 min. The supernatant was collected, evaporated and the dried sample was reconstituted with the mobile phase, filtered with 0.2μm nylon membrane filter before analysis. The brain concentration time was evaluated by pharmacokinetic software (Microsoft Excel, Pharsight Corporation, Mountain View, CA).

6.1.3 In vivo anti-glioma activity

To evaluate the in vivo anti-glioma activity of three different nanosystems, intracranial glioma-bearing rats were divided into five groups which were administered intranasally with saline (controls), free temozolomide (TMZ), TMZ loaded in PLGA-PEG NPs, TMZ loaded in mAb-PLGA NPs and TMZ loaded in Chitosane NPs. For all nanosystems a dose of 5 mg/kg of TMZ was calculated. Administrations were performed at 6, 7, 8, 9, and 10 days after C6 cell implantation. On the 15th day, one rat from each group was sacrificed, and the brain was isolated to prepare paraffin sections. The other rat (one per group) was used to calculate survival times.

6.2 Results

6.2.1 TMZ brain concentration

The concentration of TMZ in brain was estimated on the 15th day after C6 cell implantation in all groups after administration of formulations. The concentration of TMZ in brain after administration of TMZ-Chitosane was found to be significantly higher than TMZ-PLGAPEG NPs (Table 4). Conversely, administration of TMZ loaded in mAb-PLGAPEG NPs generates a lower brain concentration of TMZ compared to TMZ-PLGAPEG NPs

This result indicated that the presence of lipid and chitosane in the formulation act as a permeation enhancer and adhered for a longer period of time. The addition of chitosan as mucoadhesive polymer plays an important role in enhancing the brain uptake by giving prolonged contact time with mucosa. The higher brain concentration was achieved with TMZ-Chitosane NPs compared to TMZ-PLGAPEG NPs, showing the superiority of Chitosane as enhancer for the brain delivery by intra-nasal route. Despite the adjunct of monoclonal antibody has been conceived to potentiate brain targeting, the concentration of temozolomide in the rat treatetd with TMZ-mAb-PLGAPEG NPs was lower compared to TMZ-PLGAPEG NPs. These results are similar to those reported in the literature on nose-to-brain delivery of particle up to 200 nm in diameter (43). The administration of drug by intranasal route effords the olfactory and trigeminal nerve for drug transport from nasal epithelium to brain, bypassing BBB, which may not take place with the administration of other routes (44).

6.2.2. Evaluation of anti-glioma activity

Glioma-bearing rats were used to evaluate the anti-glioma effects of different nanosystem we tested , the survival times were 15 days for rat treated with TMZ-Chitosane NP, 16 days for rat treated with saline, 17 days for rat treated with free TMZ, 19 days for rat treated with TMZ-PLGAPEG NP, and 20 days for rat treated with TMZ-mAb-PLGAPEG NP. The short survival of rat treated with TMZ-Chitosane NP can be interpreted as the result of a toxic effect of Chitosane or TMZ on normal brain. Indeed, a similar survival time was observed in rat treated with free TMZ.

Compound adminestered	**Brain Concentration** (ng/ml)	**Survival** (days)
Saline	0	16
Free TMZ	3124.43	17
TMZ-mAb-PLGAPEG NPs	932.49	20
TMZ-PLGAPEG NPs	1639.31	19
TMZ-Chitosane NPs	2437.34	15

Table 4: Brain concentration and anti-blastic efficacy of nanosyistems tested

7. Discussion

7.1 Strategies to improve surgical and clinical outcome

Extent of tumor resection is a survival predictor in brain tumor surgery (45). The role of surgery in the multidisciplinary management of HGG, particularly in increasing time-to-progression and overall survival, has been clearly demonstrated and several evidences have been published (46,47). However, HGG have intrinsic radiological, histological, anatomo-pathological and biological heterogeneity, which make difficult the oncological approach. Indeed, HGG, often identified as the most infiltrating and aggressive tumors, are likely to be considered as the manifestation of a complex process of tumorigenesis involving not only the "visible" tumor but also the peritumoral areas.

For several years, glioblastoma peritumoral areas have been considered as regions of tumor infiltration, where tumor cells could be found intermingled with normal brain tissue. According to the commonly used neuro-oncological protocols, such areas are targeted by radiation therapy, and temozolomide-based chemotherapy can act as a cytostatic agent.

In routine neurosurgical practice, resection of HGG aims to safely remove all the visible tumor respecting neurological functions. However, all strategies aiming to increase the EOR in brain tumor surgery (i.e. 5-ALA, intraoperative imaging tools) have the potential risk to resect eloquent brain, particularly in infiltrating areas. Indeed, the old concept of neuro-oncological surgery stating that "where there is tumor, function is not present" has been definitely deny by the evidence that tumor cells infiltrating normal white matter are often identified in the context of functioning cortical areas and subcortical pathways (6,48).

Recently, the role of 5-ALA in detection of infiltrating tumor areas has been investigated. Lau et al., published in 2016 a prospective phase II clinical trial, which correlated cellularity with fluorescence

intensity in high-grade brain gliomas. This study demonstrated a direct correlation between 5-ALA fluorescence intensity and rate of gliomas′ infiltration. Interestingly, in the same study, authors highlighted some limitations in the use of 5-ALA, which can generate false positive, particularly in peritumoral areas (49).

Intuitively, resection of peritumoral areas of glioblastoma should have a positive impact on survival parameters and delay recurrence, as the increased cytoreductive effect of the so-called supramaximal resection could improve survival. Evidences on the positive correlation between tumor resection pushed beyond the margins of enhancing tumor are coming from recently published studies. Eyupoglu et al. reported the results of a series of patients undergone supra-complete resection of glioblastoma, based on 5-ALA vaguely positive areas surrounding enhancing tumor. They found prolongation of survival associated to supra-complete resection of all 5-ALA positive areas, including vaguely fluorescent ones (50).

In 2015, Li et al. published the results of a retrospective analysis on a large cohort of patients undergone surgery for HGG (51). They performed a review of 1229 operated cases, finding that gross total resection (i.e.: complete resection of enhancing tumor) was achieved in 71% of cases (876 patients). A subgroup of these patients, received a resection of ≥53.21% of the surrounding FLAIR abnormality beyond the 100% contrast-enhancing resection. In such subgroup a significant prolongation of survival, compared with that following only resection of enhancing tumor, has been documented by authors. The paper by Li et al. is important because it introduced for the first time the concept of resection of FLAIR-positive abnormalities surrounding the enhancing tumor. Nevertheless, this study lacks of a volumetric evaluation of EOTR of FLAIR-positive areas and such supramaximal resection has been only retrospectively analyzed and documented. Volumetric assessment of resection, in modern neuro-oncology, is considered the most accurate method to objectively evaluate EOTR and it should be applied not only for research purposes but also for routine clinical use, as recently highlighted by Henker et al (52).

Our study introduces a surgical protocol aiming to obtain an aware and quantifiable supra-maximal resection of glioblastoma. Stating the limits of 5-ALA focused on by Lau (49) and the promising results coming from the other reported clinical experiences, we hypothesized that neuronavigation of FLAIR sequences and pre-operatively planning of FLAIR-based resection represent a more reliable approach to guarantee a safe and accurate supra-maximal resection.

FLAIR sequences have been studied and applied to low-grade tumour pre- and post-operative evaluation for several years. Nowadays, the role of FLAIR images role in surgical planning of HGG is emerging (53,54). The usefulness of FLAIR sequences depends on the suppression of CSF artefacts, particularly in cases of cortical-subcortical lesions, having a wide extension and involving

more than one lobe or periventricular areas. In particular, FLAIR sequences are used in high-grade gliomas for radiotherapy planning, although different problems are known: radiation effects, reduction in corticosteroid doses, demyelination, ischemic injury and other post-treatment effects, may alter the tumour volume evaluation (53). Similar problems are evaluated for pre-surgical planning: if FLAIR sequences are optimal to evaluate volumes and growth of LGG, in HGG the major problem is represented by the peri-tumoral oedema, a problem known from the beginning in FLAIR use (53). Perilesional margins, not comprised in a T1 gadolimium-enhanced sequence, are composed by a mass-reactive oedema and a low-density tumour-cells infiltration. The greatest problem is the inability of FLAIR to clearly distinguish the second component from the first one (55). Different studies have tried to solve this issue, improving details of radiological acquisition techniques and their elaboration, also trying to create an auto-elaborating software to investigate the grade of tumour infiltration and follow the evolution post of neuro-radiological features (54,55).
In our series, the FLAIR segmentation has been verified evaluating the differences of MR signal detected by multiple ROIs placed in peritumoral areas. This method has been validated and used also in radiosurgery (54), demonstrating a good reliability in definition of tumoral infiltration pathway.
The application of volumetric assessment as well as the precise definition of boundaries of FLAIR positive tumor, are likely associated to a more accurate pre-operative planning and post-operative evaluation of resection. Indeed, our results, albeit limited to a small cohort, seem to demonstrate the existence of a direct and constant correlation between the extended tumor resection, which also includes peritumoral infiltrating areas, and survival. In particular, we found that a higher percentage of FLAIR based EOTR is related to a prolonged Overall Survival. This suggests a possible positive impact of the proposed protocol on clinical outcome.
Another interesting finding of our study is the results of analysis of residual tumor evaluated by FLAIR images. As demonstrated by recent evidences (56), residual tumor is a negative predictor factor of survival in glioblastoma and a residual tumor volume smaller than 2 cm^3 can guarantee a meaningful increase of clinical outcome. We performed a volumetric evaluation of residual tumor both on T1 gadolinium-enhanced and on FLAIR sequences. We did not find statistically significant correlation between residual tumor measured by T1 nor by FLAIR sequences and survival. However, the statistical strength of correlation resulted higher for FLAIR evaluated residual tumor volume. This finding is explainable as a complete (i.e.: 100% of EOTR) resection of FLAIR contoured tumor is often not achievable (to preserve neurological functions) also in most of cases harbouring 100% of T1 enhaning tumor resection.

We did not include in our analysis data concerning biomolecular asset of tumors, as such data were not available for all patients. However, correlation and regression analysis used for statistical interpretation of our data has been conceived to investigate the independent role of FLAIR-based resection in improvement of clinical parameters, regardless of other patients′ related factors.

7.2 Strategies to increase the effectiveness of adjuvant therapy: nanotechnologies to overcome BBB

The heterogeneity of GB, in combination with its high infiltrative nature, determine a poor outcome for standard treatments. To overcome these hurdles, different targeting strategies have been adopted for developing effective nanostructured delivery systems (NDS) to the brain. There are many strategies described to direct NPs to the brain tumor, including the use of nanotechnology coupled with passive, active or stimuli responsive targeting approaches (57-61).
Nanotechnology provides endless opportunities in the area of cancer treatment using targeted anticancer drug delivery systems. For that, NPs have to be appropriately studied and designed to accomplish the greatest therapeutic and/or diagnostic effect with reduced side effects, especially for chemotherapy drugs (62). NPs are complex drug delivery systems, which can be structurally divided into the external layer (shell) and internal layer (core). The shell can be functionalized with a variety of small molecules, polymers, polysaccharides, proteins and metal ions; the core, a central part of the NPs, can be chemically combined with different materials. NPs are flexible and versatile, with an architecture that ensure small size, appropriate shape, and surface functionalization, in order to accomplish the objectives of the proposed function. NPs have been shown to improve pharmacokinetics of available drugs, by reducing drug biodistribution to non-target compartments, delivering the adequate amount of the drug into the right site, overcoming solubility and stability issues and allowing higher drug encapsulation. Regarding the complexity of BBB and/or BBTB, NPs offer the possibility to encapsulate hydrophilic anticancer drugs, increase the blood circulation and tissue distribution, with improvement of their preferential accumulation at the tumor site. Additionally, NPs have been described to overcome multi-drug resistance mechanisms. Several nanostructured delivery systems (NDS) have been developed for brain tumor delivery, and depending on the nature and composition, they can be classified as organic NPs and inorganic NPs (63). Organic NPs are described as being composed by organic compounds, including lipids, surfactants or polymers with the GRAS (generally regarded as safe) status, that offer an easy way

for the encapsulation of molecules.

Liposomes, polymeric nanoparticles, lipid nanoparticles, micelles/polymeric micelles, protein based nanoparticles are some examples of organic NPs. An extensive research is already reported with organic NPs for the GB treatment. The NPs performance has been assessed through in vitro and in vivo studies, and compared with the free drugs, and the results seem to be promising, showing the ability to transport drugs across the BBB in a more efficient way, with a preferential distribution in the brain (64). On the other hand, inorganic NPs contain a solid core with physicochemical properties that can be attributed to their inorganic components, such as magnetic metal oxide or semiconductor material. Different types of inorganic NPs have been described and employed for biological applications, including iron oxide nanoparticles, mesoporous silica nanoparticles, gold nanoparticles and quantum dots. The main advantages of inorganic NPs are their robustness, resistance to enzymatic degradation and interesting intrinsic characteristics, such as optical, thermal , magnetic and electrical properties, that can be used for imaging and therapeutic approach. Considering their nature composition, inorganic NPs can be synthesized and modified in a way that facilitates the surface functionalization by incorporation of ligands or polymers, improving their biological function (65). The use of biocompatible coatings has shown to reduce the toxicity associated to the presence of the heavy metal. Inorganic NPs have also been widely investigated for diagnostic applications, using their distinct abilities to respond to external stimuli and physiological changes (66). As shown in different reviews, several types of NPs (magnetic, fluorescent, liposomal , polymeric, lipidic, among others) have already been designed and developed for crossing the BBB to GB therapy, considering passive, active and stimuli targeting approaches [67]. NPs are an interesting drug delivery system, presenting a high potential for improving patient outcomes. However, their translation from pre-clinical proof of concept to the demonstration of therapeutic value in the clinic remains a long, costly, and challenging path. The scaling up procedure, surface modification, biopersistence and toxicological aspects, recognition and quantification of NPs in the human body are some critical points that make difficult the translation. Several types of research focusing on NPs characterization, and in vitro and in vivo studies have been carried out, but many questions remain without answers. In vitro and in vitro studies for GB treatment, encompassing multiple biological targets, have been described and include gold nanoparticles, chitosan-based nanoparticle, curcumin-loaded PLGA-DSPE-PEG nanoparticles, curcumin-loaded RDP-liposomes, hyaluronic acid been evaluated in clinical trials, and fewer were extended to clinical practice (68). In what follows, the reference of clinical trial is quoted, as extracted from clinicaltrial.gov. REF Nanoliposomal CPT-11 (NCT00734682 and NCT02022644), SGT-53 (liposomal nanocomplex encapsulating a wild type p53 DNA sequence) used in combination with temozolomide, NU-0129 (

NCT03020017, gold nanoparticles based on spherical nucleic acid) and PEGylated liposomal DOX (NCT02766699, CaelyxTM, PEG-Dox) constitute some of the clinical trials that have been conducted in recent years, and illustrate the variety of theranostic approaches. NanoTherm (Aminosilane-coated SIONPs) and Opaxio (ester conjugate of − poly(L) − glutamic acid (PGA) and paclitaxel) are NPs already implemented in clinic. However, the inability to effectively control the behavior of NPs inside the body, including biodistribution, toxicity and pharmacokinetics, represents a major limitation for using nanotechnology to diagnose and treat cancer (69). Passive targeting resorts to brain tumor properties, including hyper-vascularizing, leaky and scarce lymphatic drainage system, to make drug available into the intratumoral space, while depriving healthy brain tissue. NPs dynamics through the brain depend on the integrity of the barrier, which may be compromised in the presence of some diseases, and on the size, geometry and surface properties of the actual particles. These parameters must be controlled to avoid uptake by the reticuloendothelial system (RES). To maximize circulation times and targeting ability, literature indicates NPs optimal size as less than 100 nm in diameter, and suggests the presence of an hydrophilic surface to circumvent clearance by macrophages within the RES (70). Nanoparticles 100−400 nm in size did not show significant difference for overcoming the BBB. However, significant differences were observed when nanoparticle size was below 100 nm, for which the effects were more pronounced (71). Some work focused on correlating the size of NPs to their biological effects (72). It can be concluded that the size and the charge of nanoparticles are controversial in the effects promoted in vivo, and further studies are needed to clarify this subject. Thus, NPs have the advantage of the small size to provide a preferential accumulation at the site of brain tumor due to the morphology and permeability of the barrier, EPR effect (73). The EPR effect does not occur with the conventional chemotherapeutic molecules, due to the lack of specificity between normal and tumor tissues. However, the ability of drug diffusion is an important parameter that hinders the passive targeting strategies, due to the difficulty to control drug release. Therefore, to achieve an efficient EPR effect, NPs should be smaller than 100 nm and present a biocompatible surface (neutral charge and hydrophilic properties) to avoid the reticuloendothelial system (RES) (74).

To increase the selectivity of drug release at the chosen sites of action, and achieve enhanced therapeutic efficacy, an active targeting approach is required (75). These strategies consist in incorporating affinity molecules or taking advantage of influx transport systems expressed within the BBB/BBTB, into NPs surface, bearing in mind the specific characteristics of abnormal tissue, e. g., the differential expression of receptors or antigens in cancer cells. These include a wide range of peptides, antibodies or antibody fragments, aptamers and other small molecules. Glioblastoma is

characterized by several molecular mechanisms of chemoresistance, so the development of actively targeted NPs to surface cell markers, signalling pathways and tumor microenvironment represents an interesting and challenging opportunity. These approaches are accomplished by connecting specific ligands to the NPs structure, which allows a selective recognition of different receptors overexpressed in the tumor cell surfaces. The functionalization of the NPs surface improves therapeutic efficacy of cytotoxic drugs and overcomes the multidrug resistance (MDR).
The lack of control over drug release has prompted the development of NPs tailored to respond to endogenous and/or exogenous stimuli. The benefits of internal-stimuli responsive NPs are evident, because the stimuli specifically exist in characteristic pathological sites (76). The endogenous triggers, such as pH variations, enzymes, glucose or redox gradient, can be used depending on the disease pathological characteristics (77). Tumors have an acidic pH in contrast to the normal tissues , so there is an opportunity to use pH-stimuli responsive NPs. Due to their conformation changing or bond cleavage sensitive to different pH values, pH-responsive NPs allow the release of loaded drug in precise locations. This strategy has been applied by different research groups, and the results have been satisfactory. The redox-sensitive NPs are used also as a stimuli response, due to the intrinsic redox gradients in the cells. Taking advantage of the higher concentration of glutathione (GSH) that regulates the intracellular redox condition, NPs with disulfide bonds are broken down and the cargo is released. This bond is unstable in high concentrations of GSH, being reduced to thiol groups inside the cells. The enzymatic-stimuli response is also an interesting approach, due to the high expression of enzymes in the tumor bulk, in particular extracellular matrix metalloproteinases (MMPs) (78). In turn, the exogenous triggers use external forces, including temperature, magnetic field, ultrasound, light, electric pulse, or high radiation. Targeting moieties can be combined directly or indirectly by covalent or non-covalent linkage. The heterogeneity in the physiological conditions, the combination of endo- and exogenous stimuli-responsive NDS might be more favorable, allowing to target different environments. It is possible to combine triggers, such as pH/temperature, pH/redox, temperature/redox, and temperature/pH/redox, among others, which exhibit additional advantages in comparison to NDS employing single stimulus. This is a field that has attracted much attention in recent years.

7.3. Theranostics

The current progress in GB therapy and detection evidences that there has been no significant reduction in GB associated with death rates. The heterogeneity of the tumor, the unspecific drug

delivery, the diagnosis failure in the primary stage detection are some of the reasons responsible for the treatment inefficiency. Thus, the combination of earlier detection and targeting therapy procedures, termed as theranostics, has been developed as a strategy to improve the GB treatment. The theranostic approach make possible to diagnose the GB, understand the location of the GB and the stage of disease, and also to percept the tumor progression. These strategies help to address the intra- and interpatient heterogeneity of GB, pointing out to a future application in personalized medicine. The use of a single and multimodal system appears to be one of the most promising characteristics of NPs application.

In this context, a new technological concept has been introduced and designed as theranostic nanoparticles (TNPs). TNPs are described as a combination of both organic and inorganic NPs to obtain multiple synergistic properties in a single NP, taking advantages of the drug delivery by organic NPs and imaging prompted by inorganic NPs (79). The preparation methods and physicochemical characterization through in vitro evaluation on cell culture and in vivo studies have been described for a variety of TNPs. These NPs have shown interesting results during in vitro studies.

However, considering the different diagnostic approaches, including magnetic resonance imaging (MRI), computed tomography (CT), ultrasound, optical imaging (OI) and photoacoustic imaging (PAI), positron emission tomography (PET) and single photon emission CT (SPECT), there are still some challenges for their application in vivo. The imaging modalities are based on diverse physical principles, considering the method that allows the higher sensitivity and specificity to tissue contrast, quantitative and tissue penetration, and spatial resolution. Consequently, the TNPs concept needs an extensive in vivo investigation before their clinical translation.

Indeed, several inorganic and organic NPs utilized in the diagnosis and drug delivery have been developed for different applications. Theranostic nanoparticles have shown attractive results in in vitro studies, but there are still some challenges for their application in vivo. For this reason, the major part of the research that has been described in the literature is about the preparation and characterization of TNPs with application in in vitro cell culture, still lacking the in vivo proof of concept. In the case of the treatment of human brain cancers, TNP have been developed (80), taking advantage of the specific GB characteristics described in the following sections. Gold and iron oxide-based nanoparticles have prompted particular attention as theranostic anti-cancer agent systems, combining in the same NPs drug delivery, imaging, and therapy (81). Thus, TNPs can be used to avoid frequent and invasive dosing and improve patient compliance. Recently, a research group combined chemo-photothermal targeted therapy of glioma within one nanoparticle. A targeting peptide (IP)-modified mesoporous silica-coated graphene nanosheet (GSPI) was

synthesized and characterized. Doxorubicin (DOX) was used as therapeutic component and GSPI nanoparticles as drug and diagnostic delivery system, integrating the response to heat and pH-stimuli. Only in vitro studies were performed and the results showed a higher rate of death of glioma cells and improved accumulation of GSPID (82). In another work (83), targeted TNPs were developed, which included newer (small interference RNA, siRNA) and conventional (temozolomide, TMZ) therapeutics. To promote the targeting to glioma cells, chlorotoxin (CTX) peptide was conjugated with iron oxide nanoparticles that worked as drug carrier and allowed to monitor the changes in tumor volume by magnetic resonance imaging (MRI). TNPs were internalized by T98G glioblastoma cells in vitro leading to the enhancement of TMZ toxicity. The results in vivo indicated that the combination of the treatments with the TNPs loaded with TMZ led to significant retardation of tumor growth, as monitored by MRI. The multiple emulsion solvent evaporation method has been proposed as effective for high co-encapsulation of SPIONs and DOX into the poly (lactic-co-glycolic acid) (PLGA)-based NPs. A different strategy was designed, taking advantage of magnetic nanoparticles and polymeric materials for potential application in targeted therapy and imaging of malignant tumors. Thus, SPIONs and DOX were entrapped in the PLGA nanoparticles via a modified multiple emulsion solvent evaporation method. The NPs displayed an increased DOX release at pH 5.5 compared to pH 7.4; the targeted NPs enhanced cellular uptake of DOX in C6 glioma cells, exerting a higher cytotoxic effect when compared with DOX solution alone (84).

Taken together, TNPs may lead to an improved therapeutic efficacy over DOX solution in glioma tumor growth inhibition for therapeutic and diagnostic purposes. Considering a similar strategy, chitosan NPs used as a dual action carrier for DOX (as chemotherapeutic agent) and superparamagnetic iron oxide nanoparticles (SPIONs; as imaging agent) were developed (85). The TNPs demonstrated a pH-sensitive drug release profile with a burst release at acid tumor environment. TNP-DOX were internalized and the in vitro magnetic resonance imaging (MRI) showed a decline in T2 relaxation times by increasing iron concentration. The imaging method also confirmed uptake of TNPs at the optimum concentration in C6 glioma cells. Gold nanoparticles (AuNPs) and superparamagnetic iron oxide nanoparticles (SPIONs) were combined in a unique NPs to deliver therapeutic and diagnostic agents for brain tumors. The potential applications of novel gold and SPION-loaded micelles (GSMs) coated by polyethylene glycol-polycaprolactone (PEG-PCL) polymer was also tested [385]. The results showed, by quantifying gh2ax DNA damage in GB cell lines, the radiosensitizing efficacy of these GSMs, and found that GSM administration in conjunction with radiation therapy led to ~2-fold increase in density of double-stranded DNA breaks. GSMs used as a contrast agent for the MRI studies were sensitive to detect and delineate

tumor borders. These results indicated that GSMs may potentially be integrated into both imaging and treatment of brain tumors, helping a theranostic purpose as both an MRI-based contrast agent and a radiosensitizer. Hollow gold nanospheres (HAuNS) have demonstrated an intense photoacoustic signal and induced an efficient photothermal ablation (PTA) therapy (86). According to the in vivo results, these hybrid NPs significantly prolonged the survival of tumor-bearing mice. The results revealed the feasibility of the NP image-guided local tumor PTA therapy using photoacoustic molecular imaging. The application of multitargeting in a single NPs has also been described, and some examples are mentioned. Targeting AuNPs with two or more receptor binding peptides for glioblastoma treatment have been developed. AuNPs conjugated with peptides against both the epidermal growth factor and transferrin receptors, and also loaded with the photosensitizer phthalocyanine 4 (Pc 4) was studied and compared with AuNPs employing in vitro and in vivo studies. The dual-targeting hybrid nanoparticles displayed a synergistic effect in human glioma cells and showed a significant accumulation in the brain tumor regions in in vitro studies and in vivo studies, respectively.

The ability to perform multiple functions in biological systems, toxicity and biodistribution are the main requirements for the clinical translation of nanotheranostic concept. In general, the regulatory approval of NPs is challenging, due to their higher complexity as NDS. When TNPs, as multifunctional nanocarriers, are considered, the approval process has shown to be even more complicated, involving therapeutic, diagnostic and targeting agent assessments.

7.4. Personalized Medicine

Personalized medicine considers the pharmacogenetics, pharmacogenomics and pharmacoproteomic information as crucial for the prescription of therapeutics directed at each patient (87). Thus, this new field considers the variability of each individual before developing an appropriate treatment strategy. The application of personalized medicine in the oncology field displays a promising strategy, due to the better understanding of the disease at a molecular level. Personalized medicine may be effective in the treatment and/or control of cancers with the implementation of a high specificity and accuracy of diagnosis (88). Thus, the optimization of the treatment protocols becomes simpler and less expensive, associated with fewer toxicities and a high efficacy. Personalized cancer medicine (PCM) is defined as treatment based on the molecular characteristics of a tumor from an individual patient (89). Recent researches have clarified several cellular and molecular mechanisms of tumor development, growth and metastasis with the identification of new cancer specific molecular targets. Taking advantage of pharmacogenetic,

pharmacogenomic, pharmacoproteomic strategies, the detailed genetic and molecular profile of each patient, personalized medicine can help tailoring the design of nanoparticles. Targeted nanoparticles can interact with specific molecular biomarkers, which determine the evolution of the disease and the response to treatments (90). Nanoparticles used in the personalized medicine are optimized treatment to each patient, taking into account the individual variability. However, critical steps are important in the personalized cancer therapy development, including a comprehensive assessment of biological characteristics of tumors from each individual and validated methods to identify the groups or subgroups of patients with more benefits in that therapy. Personalized medicine applied to a cancer presents a good example of a therapy relying on the individual genotype. The main difficulty in the translation to the clinic of nanoparticles in the context of personalized medicine is that it requires a comprehensive and detailed understanding of the potential toxicological risk associated to their use. If this difficulty can be overcome, clinical application of nanoparticles would allow to detect variation among patients, thus driving the clinical decisions and the elaboration of therapeutic protocols.

The GB heterogeneity, their invasiveness and the numerous mutations, contribute to the progression of the tumor and the treatment failure (91). Due to the different patient responses to conventional oncological treatments, the use of nanotechnology associated with personalized medicine is promising for the improvement of current strategies and the success of the treatment. Targeting tumor heterogeneity and immune system may be applied using multifunctional nanoparticles, which may help prevent recurrence in GB by specific eradication of tumor cells. TNPs can permit the co-development, in single nanoparticles, of therapy, imaging and targeting approach, matching the most effective treatment to the individual patient.

Thus, it is predicted that personalized medicine along with the knowledge of GB environment with use of TNPs will improve their therapeutic and diagnosis efficacy. TNPs for personalized medicine will emerge and enter clinical trials. However, before this becomes a reality, safety concerns, problems related to the maintenance of robustness and reproducibility in the up-scaling processes must be addressed.

7.5. Preclinical phase and clinical trials

As it has been discussed, NPs are promising for applications in cancer theranostics because of their affinity and selectivity to tumor cells. In addition, they can simply be surface modified to increase their blood circulation times and make them functionalized with active targeting ligands. Recent advances in TNPs research have resulted in a number of formulations containing both drugs and

imaging agents within a single formulation. However, despite the progress in the TNPs, their translation to the market has been a challenge. There are some researches focused on the preclinical trial phases, studying essentially the toxicity, pharmacodynamics, and safety profile of the TNPs. The main studies occur in vitro and in vivo, establishing the knowledge about the effect of a wide range of NPs doses to be tested, using cancer cell lines versus normal cell lines, and, as in a second step, in vivo assessment with appropriate animal models. Here, it is possible to evaluate the biocompatibility and the behavior of NPs with direct relation with the animal. The main purpose of the preclinical trials is to move forward the TNPs from the preliminary stage to the clinical phase. Theranostic NPs, that combined organic nanoparticles (including liposomes, micelles/polymeric micelles, lipid nanoparticles, protein based nanoparticles) with co-delivery of drugs, and inorganic NPs (e.g., QDs, gold nanoparticles, and silica nanoparticles) as imaging contrast, have been developed and the major part of the results displayed a higher effectiveness than the commercial references (92-100).

The explosion of NPs for clinical imaging and therapy has not occurred yet. Their higher complexity and dubious reproducibility will create significant hurdles for clinical translation and regulatory approval. Although there are described several organic NPs for treatment and inorganic NPs for theimaging application approved or in clinical trials, these approaches did not represent a theranostic approach. INFeD®, DexIron®/Dexferrum Feridex®, FerahemeTM (Ferumoxytol), NanoTherm®,

Venofer®, AuroLase Therapy and AuNPs-nanosensor are some inorganic nanoparticles in current clinical trials or approved. Only NanoTherm® is an intratumoral thermotherapy used for GB treatment, and the treatment is based on the principle of introducing magnetic nanoparticles directly into the tumor and then heating it using an alternating magnetic field (101). A minimally invasive surgical procedure is used to introduce the magnetic fluid into the tumor followed by placing of the thermometry catheter in the treatment area to allow direct measurement of the temperature during thermotherapy. Although there are several TNPs under development, most of them do not yet possess a preclinical proof of concept, due to failure in the correlation between the in vitro and the in vivo results.

8. Limitations and perspectives

Both clinical and pre-clinical experience and experiments reported in this thesis have several limitations: clinical study is based on a single centre experience and results are preliminary with some patients still alive and under follow-up. This makes clinical data not conclusive, despite our experience suggests a positive impact of technologies on patient survival. Similarly results of in vivo experiments are based on a very limited number of rats and we had not the possibility to make statistical analysis. However, all the experiments confirmed the possibility to apply nanotechnologies to research on brain tumors and can constitute a cue for further research on this field.

The message and the meaning of our pre-clinical and clinical experiments is that a translational approach to glioblastoma is likely the key to improve the care of such a terrible disease. Surgical efforts must be made to "clean" the brain as much as possible from tumor cells without causing neurological deficits to the patients. On the other hand, researches on adjuvant therapies to prevent

or delay recurrences should be performed. In this direction, studies on nanosystems and targeted therapies are encouraged as glioblastoma should be finally treated as a disease involving the entire brain and not as a tumor. However, the most difficult step to overcome is probably represented by the challenges related to the translation from laboratory to the hospital of researches on new compounds. An animal model of glioblastoma is definitely far from the clinical reality and there are not yet available designed clinical protocols on TMZ combined with nanodrugs which can be administered intranasally.

9. Conclusions

GB is one of the most dismal and mortal diseases, with no effective treatment. The BBB and BBTB , as the main physiological barriers, heterogeneity and the invasive nature of GB, lead to an inadequate concentration of chemotherapeutics at the site of tumor, restricting current treatments. These difficulties can be overcome using nanotechnology, which has demonstrated to be an opportunity in the area of cancer treatment. Thus, the NPs utilization may lead to a breakthrough in brain cancer management, due to their small size, high surface functionalization and, more recently, the opportunity to co-develop treatment and imaging in a single NP. In this review, it is shown that optimization of NPs in theranostics is a multivariable, multi-objective task that does not allow to point in a single direction. Theranostic NPs are smart carriers, able to diagnose, deliver and monitor the therapeutic response in real-time. Targeting overexpressed proteins and receptors on brain

cancer cells allows a specific release of cargo in the exact site. The knowledge about the chemotherapeutics concentration and safer pharmacokinetic profiles, with a real-time monitoring of biodistribution and target site accumulation, visualization of the target receptor density and assessment of the therapeutic efficacy may be beneficial in the selection of therapy and planning the treatment. In the coming years, the global perspective for the use of TNPs is clearly optimistic, in multifunctional applications and in combination with personalized medicine strategies, offering hope for their successful clinical translation. Providing treatment at the right time depends on right-time diagnosis. Personalized cancer planning, advance diagnosis, and suitable drugs for the right patient, with predictable side effects, can finally make this goal a reality. Modern multimodality treatment and care increase patient′s life quality and life expectancy. It is probable that, in the next years, TNPs will emerge and enter clinical trials.

References

1. Ostrom QT, Gittleman H, Liao P, et al. CBTRUS Statistical Report: Primary Brain and Central Nervous System Tumors Diagnosed in the United States in 2008-2012. Neuro Oncol . 2015;16 Suppl 4(suppl_4):iv1-iv63.

2. Brown TJ, Brennan MC, Li M, Church EW, Brandmeir NJ, Rakszawski KL. Association of the extent of resection with survival in glioblastoma: a systematic review and meta-analysis. JAMA oncology. 2016; 2(11): 1460-1469.

3. Hervey-Jumper SL, Berger MS. Maximizing safe resection of low-and high-grade glioma. Journal of neuro-oncology 2016; 130(2): 269-282.

4. Walker MD, Alexander E, Hunt WE, et al. Evaluation of BCNU and/or radiotherapy in the treatment of anaplastic gliomas. J Neurosurg. 1978;49(3):333-343.

5. Walker MD, Green SB, Byar DP, Alexander E BU, WH B. Randomized comparisons of radiotherapy and nitrosoureas for the treatment of malignant glioma after surgery. N Engl J Med. 1980;303:1323-1329

6. Sala F, Lanteri P. Brain surgery in motor areas: the invaluable assistance of intraoperative neurophysiological monitoring. J Neurosurg Sci. 2003; 47: 79–88.

7. Jankovski A, Francotte F, Vaz G, Fomekong E, Duprez T, Van Boven M, Docquier MA, Hermoye L, Cosnard G, Raftopoulos C. Intraoperative magnetic resonance imaging at 3-T using a dual independent operating room-magnetic resonance imaging suite: development, feasibility, safety, and preliminary experience. Neurosurgery. 2008; 63(3): 412-426.

8. Senft C, Franz K, Ulrich CT, Bink A, Szelényi A, Gasser T, Seifert V. Low field intraoperative MRI-guided surgery of gliomas: a single center experience. Clinical neurology and neurosurgery. 2010; 112(3): 237-243.

9. Senft C, Seifert V, Hermann E, Franz K, Gasser T. Usefulness of intraoperative ultra low-field magnetic resonance imaging in glioma surgery. Neurosurgery. 2008; 63(4 Suppl 2): 257-267.

10. Barbagallo GM, Palmucci S, Visocchi M, Paratore S, Attinà G, Sortino G, Albanese V, Certo F. Portable intraoperative computed tomography scan in image-guided surgery for brain high-grade gliomas: analysis of technical feasibility and impact on extent of tumor resection. Operative Neurosurgery. 2015; 12(1): 19-30.
11. Eboli P, Shafa B, Mayberg M. Intraoperative computed tomography registration and electromagnetic neuronavigation for transsphenoidal pituitary surgery: accuracy and time effectiveness. J Neurosurg. 2011; 114(2): 329-335.

12. Hosoda T, Takeuchi H, Hashimoto N, Kitai R, Arishima H, Kodera T, Higashino Y, Sato K, Kikuta K. Usefulness of intraoperative computed tomography in surgery for low grade gliomas: a comparative study between two series without and with intraoperative computed tomography. Neurol Med Chir (Tokyo). 2011; 51(7): 490-495.

13. Yamashita S, Fujisawa M, Kodama K, Ishikawa M, Katagi R. Use of preoperative 3D CT/MR fusion images and intraoperative CT to detect lesions that spread onto the brain surface. Acta Neurochir Suppl. 2013; 118: 239-244.

14. Kubben PL, ter Meulen KJ, Schijns OE, ter Laak-Poort MP, van Overbeeke JJ, van Santbrink H. Intraoperative MRI-guided resection of glioblastoma multiforme: a systematic review. Lancet Oncol. 2011; 12(11): 1062-1070.

15. Stummer W, Pichlmeier U, Meinel T, Wiestler OD, Zanella F, Reulen HJ, ALA-Glioma Study Group. Fluorescence-guided surgery with 5-aminolevulinic acid for resection of malignant glioma: a randomised controlled multicentre phase III trial. The lancet oncology. 2006; 7(5): 392-401.

16. Sanai N, Polley MY, McDermott MW, Parsa AT, Berger MS. An extent of resection threshold for newly diagnosed glioblastomas. J Neurosurg 2011; 115(1):3-8.

17. Kamp MA, Dibué M, Niemann L, et al. Proof of principle: Supramarginal resection of cerebral metastases in eloquent brain areas. Acta Neurochir (Wien). 2012;154(11):1981-1986.

18. Muccio CF, Tarantino A, Esposito G, Cerase A. Differential diagnosis by unenhanced FLAIR T2-weighted magnetic resonance images between solitary high grade gliomas and cerebral metastases appearing as contrast-enhancing cortico-subcortical lesions. J Neurooncol. 2011;103(3):713-717.

19. Reinertsen I, Lindseth F, Askeland C, Iversen DH, Unsgård G. Intra-operative correction of brain-shift. Acta Neurochir (Wien). 2014;156(7):1301-1310.

20. Barbagallo GM V., Paratore S, Caltabiano R, et al. Long-term therapy with temozolomide is a feasible option for newly diagnosed glioblastoma: a single-institution experience with as many as 101 temozolomide cycles. Neurosurg Focus. 2014;37(6):E4.

21. Gao J, Wang Z, Liu H, Wang L, Huang G. Liposome encapsulated of temozolomide for the treatment of glioma tumor: preparation, characterization and evaluation. Drug Discov Ther. 2015;9(3):205-212.

22. Kumari S, Ahsan SM, Kumar JM, Kondapi AK, Rao NM.Overcoming blood brain barrier with a dual purpose Temozolomide loaded Lactoferrin nanoparticles for combating glioma (SERP-17-12433). Sci Rep. 2017 ;7(1):6602.

23. Ong WY, Shalini SM, Costantino L. Nose-to-brain drug delivery by nanoparticles in the treatment of neurological disorders. Curr Med Chem. 2014;21(37):4247-56.

24. Carrie R. McDonald, Ph.D.1, 6, Nathan S. White, Ph.D.2, 6, Nikdokht Farid, M.D.2, 6 GL, Ph.D.3, Joshua M. Kuperman, Ph.D.2, 6, Hauke Bartsch, Ph.D.6, Donald J. Hagler, Ph.D.2 6, Santosh Kesari, M.D., Ph.D.4, 7, Bob S. Carter, M.D., Ph.D.5, Clark C. Chen, M.D. PD., and Anders M. Dale P. Recovery of White Matter Tracts in Regions of Peritumoral FLAIR Hyperintensity using Restriction Spectrum Imaging. AJNR Am J Neuroradiol. 2013;34(6) :1157-1163.

25. Chinot OL, Macdonald DR, Abrey LE, Zahlmann G, Kerloëguen Y, Cloughesy TF. Response assessment criteria for glioblastoma: practical adaptation and implementation in clinical trials of antiangiogenic therapy. Curr Neurol Neurosci Rep. 2013;13(5):347.

26. Ramalho MJ, Pereira MC. Preparation and Characterization of Polymeric Nanoparticles: An Interdisciplinary Experiment. Journal of Chemical Education. 2016;93,1446-1451.

27. Makadia, HK, Siegel, SJ. Poly Lactic-co-Glycolic Acid (PLGA) as Biodegradable Controlled Drug Delivery Carrier. Polymers. 2011;3,1377-1397.

28. Danhier F, Ansorena E, Silva JM, Coco R, Le Breton A, Preat . PLGA-based nanoparticles: an overview of biomedical applications. Journal of controlled release : official journal of the Controlled Release Society. 2012;161,505-522.

29. Li H, Lei B, Xiang W, Wang H, Feng W, Liu Y, Qi S. Differences in Protein Expression between the U251 and U87 Cell Lines. Turk Neurosurg. 2017;27(6):894-903.

30. Loureiro JA, Gomes B, Fricker G, Coelho MAN, Rocha S, Pereira MC. Cellular uptake of PLGA nanoparticles targeted with anti-amyloid and anti-transferrin receptor antibodies for Alzheimer′s disease treatment. Colloids and Surfaces B: Biointerfaces. 2016;145,8-13.

31. Holzer M, Vogel V, Mäntele W, Schwartz D, Haase W, Langer K. Physico-chemical characterisation of PLGA nanoparticles after freeze-drying and storage. European Journal of Pharmaceutics and Biopharmaceutics. 2009;72,428-437.

32. Gelperina S, Maksimenko O, Khalansky A, Vanchugova L, Shipulo E, Abbasova K, Berdiev R, Wohlfart S, Chepurnova N, Kreuter J,. Drug delivery to the brain using surfactant-coated poly(lactide-co-glycolide) nanoparticles: Influence of the formulation parameters. European Journal of Pharmaceutics and Biopharmaceutics. 2010; 157-163.

33. Dammer U, Hegner M, Anselmetti D, Wagner P, Dreier M, Huber W, Güntherodt HJ, Specific antigen/antibody interactions measured by force microscopy. Biophysical Journal. 1996;70, 2437-2441.

34. Musumeci, T., Ventura, C.A., Giannone, I., Ruozi, B, Montenegro, L, Pignatello R, Puglisi PLA/PLGA nanoparticles for sustained release of docetaxel. International journal of pharmaceutics. 2006;325, 172-179.

35. Wohlfart S, Gelperina S, Kreuter J. Transport of drugs across the blood–brain barrier by nanoparticles. Journal of Controlled Release. 2012;161,264-273.

36. Wu M, Fan Y, Lv S, Xiao B, Ye M, Zhu X. Vincristine and temozolomide combined chemotherapy for the treatment of glioma: a comparison of solid lipid nanoparticles and nanostructured lipid carriers for dual drugs delivery. Drug Delivery. 2015;1-6.

37. Saraiva C, Praça C, Ferreira R, Santos T, Ferreira L, Bernardino L. Nanoparticle mediated brain drug delivery: overcoming blood–brain barrier to treat neurodegenerative diseases. Journal of Controlled Release. 2016;235,34-47.

38. Veszelka S, Bocsik A, Walter FR, Hantosi D, Deli MA. Blood-brain barrier coculture models to study nanoparticle penetration: Focus on co-culture systems. Acta Biologica Szegediensis. 2015;59,157-168.

39. Masserini M. Nanoparticles for Brain Drug Delivery. ISRN Biochemistry. 2013;18.

40. Cohen S, Yoshioka T, Lucarelli M, Hwang LH, Langer R. Controlled delivery systems for proteins based on poly(lactic/glycolic acid) microspheres. Pharmaceutical research. 1991;8, 713-720.

41. Dunn KW., Kamocka MM, McDonald JH. A practical guide to evaluating colocalization in biological microscopy. American Journal of Physiology - Cell Physiology. 2011;300, C723-C742

42. Hua H, Zhang X, Mu H, Meng Q, Jiang Y, Wang Y, Lu X, Wang A, Liu S, Zhang Y, Wan Z, Sun K. RVG29-modified docetaxel-loaded nanoparticles for brain-targeted glioma therapy. Int J Pharm. 2018 May 30;543(1-2):179-189.

43. Mistry A, Stolnik S, Illum L. Nose-to-Brain Delivery: Investigation of the Transport of Nanoparticles with Different Surface Characteristics and Sizes in Excised Porcine Olfactory Epithelium. Mol Pharm. 2015 Aug 3;12(8):2755-66.

44. Crowe TP, Greenlee MHW, Kanthasamy AG, Hsu WH.Mechanism of intranasal drug delivery directly to the brain. Life Sci. 2018 Feb 15;195:44-52.

45. Brown TJ, Brennan MC, Li M, Church EW, Brandmeir NJ, Rakszawski KL, Patel AS, Rizk EB, Suki D, Sawaya R, Glantz M. Association of the Extent of Resection With Survival in Glioblastoma: A Systematic Review and Meta-analysis. JAMA Oncol. 2016 Nov 1;2(11) :1460-1469.

46. Ryken TC, Frankel B, Julien T, Olson JJ. Surgical management of newly diagnosed glioblastoma in adults: role of cytoreductive surgery. J Neurooncol. 2008;89(3):271-86.

47. Hentschel SJ, Lang FF. Current surgical management of glioblastoma. Cancer J. 2003;9(2) :113-25.

48. Elaimy AL, Mackay AR, Lamoreaux WT, et al. Clinical Outcomes of Gamma Knife Radiosurgery in the Salvage Treatment of Patients with Recurrent High-Grade Glioma. World Neurosurg. 2017;80(6):872-878.

49. Lau D, Hervey-Jumper SL, Chang S, Molinaro AM, McDermott MW, Phillips JJ, Berger MS. A prospective Phase II clinical trial of 5-aminolevulinic acid to assess the correlation of intraoperative fluorescence intensity and degree of histologic cellularity during resection of high-grade gliomas. J Neurosurg. 2016 May;124(5):1300-9.

50. EyÜpoglu IY, Hore N, Merkel A, Buslei R, Buchfelder M, Savaskan N. Supra-complete surgery via dual intraoperative visualization approach (DiVA) prolongs patient survival in glioblastoma. Oncotarget. 2016;7(18):25755-68.

51. Li YM, Suki D, Hess K, Sawaya R. The influence of maximum safe resection of glioblastoma on survival in 1229 patients: Can we do better than gross-total resection? J Neurosurg. 2016;124(4):977-88.

52. Henker C, Kriesen T, Glass Ä, Schneider B, Piek J. Volumetric quantification of glioblastoma: experiences with different measurement techniques and impact on survival. J Neurooncol. 2017;135(2):391-402.

53. Jha R, Battey TW, Pham L, Lorenzano S, Furie KL, Sheth KN, Kimberly WT.Fluid-attenuated inversion recovery hyperintensity correlates with matrix metalloproteinase-9 level and hemorrhagic transformation in acute ischemic stroke. Stroke. 2014;45(4):1040-1045.

54. Duma CM, Kim BS, Chen PV, Plunkett ME, Mackintosh R, Mathews MS, Casserly RM, Mendez GA, Furman DJ, Smith G, Oh N, Caraway CA, Sanathara AR, Dillman RO, Riley AS, Weiland D, Stemler L, Cannell R, Abrams DA, Smith A, Owen CM, Eisenberg B, Brant-Zawadzki M. Upfront boost Gamma Knife "leading-edge" radiosurgery to FLAIR MRI-defined tumor migration pathways in 174 patients with glioblastoma multiforme: a 15-year assessment of a novel therapy. J Neurosurg. 2016 Dec;125(Suppl 1):40-49.

55. Muccio CF, Tarantino A, Esposito G, Cerase A. Differential diagnosis by unenhanced FLAIR T2-weighted magnetic resonance images between solitary high grade gliomas and cerebral metastases appearing as contrast-enhancing cortico-subcortical lesions. J Neurooncol. 2011;103(3):713-717.

56. Grabowski MM, Recinos PF, Nowacki AS, Schroeder JL, Angelov L, Barnett GH, Vogelbaum MA Residual tumor volume versus extent of resection: predictors of survival after surgery for glioblastoma. J Neurosurg. 2014;121(5):1115-23.

57. Pinto MP, Arce M, Yameen B, Vilos C. Targeted brain delivery nanoparticles for malignant gliomas. Nanomedicine 2017;12:59-72.

58. Sato Y, Sakurai Y, Kajimoto K, Nakamura T, Yamada Y, Akita H, Harashima H. Innovative Technologies in Nanomedicines: From Passive Targeting to Active Targeting/From Controlled Pharmacokinetics to Controlled Intracellular Pharmacokinetics. Macromol.

Biosci. 2017;17.

59. Wang M, Thanou M. Targeting nanoparticles to cancer. Pharmacol. Res. 2010;62:90-99.

60. Wadajkar AS, Dancy JG, Hersh DS, Anastasiadis P, Tran NL, Woodworth GF, Winkles JA , Kim AJ. Tumor-targeted nanotherapeutics: Overcoming treatment barriers for glioblastoma . Wiley Interdiscip. Rev. Nanomed. Nanobiotechnol. 2017;9.

61. Lee GY, Qian WP, Wang L, Wang YA, Staley CA, Satpathy M, Nie S, Mao H, Yang, L. Theranostic nanoparticles with controlled release of gemcitabine for targeted therapy and MRI of pancreatic cancer. ACS Nano 2013;7:2078-2089.

62. Tzeng SY, Green, J.J. Therapeutic nanomedicine for brain cancer. Ther Deliv. 2013;4:687-704.

63. Bertrand N, Wu J, Xu X, Kamaly N, Farokhzad OC, Cancer nanotechnology: The impact of passive and active targeting in the era of modern cancer biology. Adv. Drug Deliv. Rev. 2014;66:2-25.

64. Liu X. Madhankumar AB, Miller PA, Duck KA, Hafenstein S, Rizk E, Slagle-Webb B, Sheehan JM, Connor JR, Yang QX. MRI contrast agent for targeting glioma: Interleukin-13 labeled liposome encapsulating gadolinium-DTPA. Neuro Oncol. 2015;18:691-699.

65. Nam J, Won N, Bang J, Jin H, Park J, Jung S, Jung S, Park Y, Kim S. Surface engineering of inorganic nanoparticles for imaging and therapy. Adv. Drug Deliv. Rev. 2013;65:622-648 .

66. Bharti C, Gulati N, Nagaich U, Pal A. Mesoporous silica nanoparticles in target drug delivery system: A review. Int. J. Pharm. Investig. 2015;5:124-133.

67. Miranda A, Blanco-Prieto MJ, Sousa J, Pais A, Vitorino C. Breaching barriers in glioblastoma. Part II: Targeted drug delivery and lipid nanoparticles. Int. J. Pharm. 2017; 531:389-410.

68. Rabane JM, Latreille PL, Lalloz A, Hildgen P, Banquy X. Chapter 4-Nanostructured Nanoparticles for Improved Drug Delivery; Elsevier Inc.: Amsterdam, The Netherlands, 2017.

69. Hare JI, Lammers T, Ashford MB, Puri S, Storm G, Barry ST Challenges and strategies in anti-cancer nanomedicine development: An industry perspective. Adv. Drug Deliv. Rev. 2017;108:25-38.

70. Blanco E, Shen H, Ferrari M. Principles of nanoparticle design for overcoming biological barriers to drug delivery. Nat. Biotechnol. 2015;33:941-951

71. Gao K, Jiang X. Influence of particle size on transport of methotrexate across blood brain barrier by vpolysorbate 80-coated polybutylcyanoacrylate nanoparticles. Int. J. Pharm. 2006; 310:213-219.

72. Tang L, Fan TM, Borst LB, Cheng J. Synthesis and biological response of size-specific, monodisperse drug−silica nanoconjugates. ACS Nano 2012;6,3954−3966.

73. Davis ME, Chen Z, Shin DM, Nanoparticle therapeutics: An emerging treatment modality for cancer. In Nanoscience And Technology: A Collection of Reviews from Nature Journals ; World Scientific: Singapore, 2010;pp. 239-250.

74. Jo DH, Kim JH, Lee TG, Kim JH. Size, surface charge, and shape determine therapeutic effects of nanoparticles on brain and retinal diseases. Nanomed. Nanotechnol. Biol. Med. 2015;11:1603-1611.

75. Mikitsh, JL, Chacko AM. Pathways for small molecule delivery to the central nervous system across the blood-brain barrier. Perspect. Med. Chem. 2014;6:11.

76. Kang T, Li F, Baik S, Shao W, Ling D, Hyeon T. Surface design of magnetic nanoparticles for stimuli-responsive cancer imaging and therapy. Biomaterials. 2017;136:98-114.

77. Lu N, Huang P, Fan W, Wang Z, Liu Y, Wang S, Zhang G, Hu J, Liu W, Niu G. Tri-stimuli -responsive biodegradable theranostics for mild hyperthermia enhanced chemotherapy. Biomaterials. 2017;126:39-48.

78. Shi NQ, Gao W, Xiang B, Qi XR. Enhancing cellular uptake of activable cell-penetrating peptide−doxorubicin conjugate by enzymatic cleavage. Int. J. Nanomed. 2012;7:1613-1621.

79. Sailor MJ, Park J. Hybrid nanoparticles for detection and treatment of cancer. Adv. Mater. 2012;24:3779-3802.

80. Bhojani MS, Van Dort M, Rehemtulla A, Ross BD. Targeted imaging and therapy of brain cancer using theranostic nanoparticles. Mol. Pharm. 2010;7:1921-1929.

81. Shevtsov MA, Nikolaev BP, Yakovleva LY, Dobrodumov AV, Zhakhov AV, Mikhrina AL, Pitkin E, Parr MA, Rolich VI, Simbircev AS. Recombinant interleukin-1 receptor antagonist conjugated to superparamagnetic iron oxide nanoparticles for theranostic targeting of experimental glioblastoma. Neoplasia 2015;17:32-42.

82. Lee JE, Lee N, Kim T, Kim J, Hyeon T. Multifunctional mesoporous silica nanocomposite nanoparticles for theranostic applications. Acc. Chem. Res. 2011:44:893-902.

83. Yoo B, Ifediba MA, Ghosh S, Medarova Z, Moore A. Combination treatment with theranostic nanoparticles for glioblastoma sensitization to TMZ. Mol. Imaging Biol. 2014; 16:680-689.

84. Mosafer J, Teymouri M, Abnous K, Tafaghodi M, Ramezani M. Study and evaluation of nucleolin-targeted delivery of magnetic PLGA-PEG nanospheres loaded with doxorubicin to C6 glioma cells compared with low nucleolin-expressing L929 cells. Mater. Sci. Eng. C 2017;72:123-133.

85. Gholami L, Tafaghodi M, Abbasi B, Daroudi M, Kazemi Oskuee R. Preparation of superparamagnetic iron oxide/doxorubicin loaded chitosan nanoparticles as a promising glioblastoma theranostic tool. J. Cell. Physiol. 2018.

86. Lu W, Melancon MP, Xiong C, Huang Q, Elliott A, Song S, Zhang R, Flores LG, Gelovani JG. Wang LV. Effects of photoacoustic imaging and photothermal ablation therapy mediated by targeted hollow gold nanospheres in an orthotopic mouse xenograft model of glioma. Cancer Res. 2011;71:6116–6121.

87. Vant′s Veer LJ, Bernards R. Personalized cancer medicine. In Encyclopedia of Cancer; Springer: New York, NY, USA, 2008; pp. 2291–2295.

88. Bode AM, Dong Z. Precision oncology-the future of personalized cancer medicine? NPJ Precis. Oncol. 2017;1.

89. Wistuba II, Gelovani JG, Jacoby JJ, Davis SE, Herbst RS. Methodological and practical challenges for personalized cancer therapies. Nat. Rev. Clin. Oncol. 2011;8:135.

90. Sau S, Tatiparti K, Alsaab HO, Kashaw SK, Iyer AK. A tumor multicomponent targeting chemoimmune drug delivery system for reprograming the tumor microenvironment and personalized cancer therapy. Drug Discov. Today 2018;23:1344-1356.

91. Weller M, Stupp R, Hegi M, Wick W. Individualized targeted therapy for glioblastoma: Fact or fiction? Cancer J. 2012;18:40-44.

92. Muthu MS, Kulkarni SA, Raju A, Feng SS. Theranostic liposomes of TPGS coating for targeted co-delivery of docetaxel and quantum dots. Biomaterials. 2012;33:3494–3501.

93. Wen CJ, Sung CT, Aljuffali IA, Huang YJ, Fang JY. Nanocomposite liposomes containing quantum dots and anticancer drugs for bioimaging and therapeutic delivery: A comparison of cationic, PEGylated and deformable liposomes. Nanotechnology. 2013;24:325101.

94. Kumar R, Kulkarni A, Nagesha DK, Sridhar S. In vitro evaluation of theranostic polymeric micelles for imaging and drug delivery in cancer. Theranostics. 2012; 2:714-722.

95. Guo J, Hong H, Chen G, Shi S, Nayak TR, Theuer CP, Barnhart TE, Cai W, Gong S. Theranostic unimolecular micelles based on brush-shaped amphiphilic block copolymers for tumor-targeted drug delivery and positron emission tomography imaging. ACS Appl. Mater. Interfaces. 2014;6:21769-21779.

96. Kuang Y, Zhang K, Cao Y, Chen X, Wang K, Liu M, Pei R. Hydrophobic IR-780 dye encapsulated in CRGD-conjugated solid lipid nanoparticles for NIR imaging-guided photothermal therapy. ACS Appl. Mater. Interfaces. 2017;9:12217-12226.

97. Sarvagalla S, Hsieh HP, Coumar MS. Therapeutic polymeric nanoparticles and the methods of making and using thereof: A patent evaluation of WO2015036792. Expert Opin. Ther. Pat. 2016;26:751-755.

98. Lee J, Jeong EJ, Lee YK, Kim K, Kwon IC, Lee KY. Optical Imaging and Gene Therapy with Neuroblastoma-Targeting Polymeric Nanoparticles for Potential Theranostic Applications. Small 2016;12:1201-1211.

99. Flores, C.Y.; Achilli, E.; Grasselli, M. Radiation-induced preparation of core/shell gold/albumin nanoparticles. Radiat. Phys. Chem. 2017;142.60-62.

100. Croissant JG, Zhang D, Alsaiari S, Lu J, Deng L, Tamanoi F, AlMalik AM, Zink JI, Khashab NM. Protein-gold clusters-capped mesoporous silica nanoparticles for high drug loading, autonomous gemcitabine/doxorubicin co-delivery, and in-vivo tumor imaging. J. Control. Release 2016;229:183-191.

101. Maier-Hauff K, Ulrich F, Nestler D, Niehoff H, Wust P, Thiesen B, Orawa H, Budach V, Jordan A. Efficacy and safety of intratumoral thermotherapy using magnetic iron -oxide nanoparticles combined with external beam radiotherapy on patients with recurrent glioblastoma multiforme. J. Neurooncol. 2011;103:317-324.